Eastward-Propagating Intraseasonal Oscillation Represented by Chikira–Sugiyama Cumulus Parameterization. Part II: Understanding Moisture Variation under Weak Temperature Gradient Balance

MINORU CHIKIRA

Research Institute for Global Change, JAMSTEC, Yokohama, Japan

(Manuscript received 4 February 2013, in final form 12 September 2013)

ABSTRACT

The eastward-propagating intraseasonal oscillation represented by the Chikira–Sugiyama cumulus scheme in a general circulation model was investigated focusing on the variation of the free-tropospheric humidity. The net effect of the vertical advection and cloud process amplifies the positive moisture anomaly in the mature phase, supporting the moisture-mode theory. The horizontal advection causes the eastward propagation of the field. The variation of the moisture profile is accurately understood by using environmental vertical velocity outside cumuli. The velocity is regulated by a thermodynamic balance under a weak temperature gradient. A nondimensional parameter α plays an important role in the moisture variation, which characterizes the efficiency of moistening (drying) induced by external heating (cooling). In the middle and lower troposphere, the major moistening factor is the radiative warming anomaly, which induces the upward environmental vertical velocity anomaly. The reevaporation of the precipitation works as drying, since its cooling effect induces the downward environmental vertical velocity anomaly. Snow melting significantly cools and thereby dries the midtroposphere. The moistening of the midtroposphere is important for moistening the lower troposphere through the reduction of α. The efficiency of moistening depends on the heating profile, and congestus clouds play an important role in it. The heating profile, which maximizes the moistening of the free troposphere, is realized in the mature phase. The atmosphere is marginally unstable even in the mature phase, which is a favorable condition for the congestus clouds to occur.

1. Introduction

The Madden–Julian oscillation (MJO) is the dominant variability in the tropical atmosphere on time scales shorter than a season (e.g., Madden and Julian 2005). It is a planetary-scale eastward-propagating mode, manifesting itself in various meteorological and oceanic fields in the tropics. Many theories have been proposed to understand the MJO dynamics and help guide model development (e.g., Zhang 2005). Although these theories succeeded in explaining some aspects of the MJO, none of them are agreed to be satisfactory in systematically representing the various observed features of the MJO. The understanding of the fundamental physics of the MJO remains controversial.

Recent studies on its mechanism brought attention to the role of free-tropospheric humidity. It has been shown that the humidity has a significant control over moist convection by both observational (e.g., Numaguti et al. 1995; Brown and Zhang 1997; Sherwood 1999) and modeling studies (e.g., Tompkins 2001; Redelsperger et al. 2002; Grabowski 2003; Derbyshire et al. 2004). Systematic theories on the equatorial waves need to consider its critical effect in some ways.

One school of thought that considers the role of the free-tropospheric humidity in the MJO is the discharge–recharge mechanism (e.g., Bladé and Hartmann 1993; Hu and Randall 1994). Based on the modeling studies, it maintained that a gradual enhancement of an instability (recharge) occurs with a certain time scale, and then it is stabilized by deep convection (discharge). Although it was originally not relevant to the humidity, the concept was later linked with a gradual increase in the free-tropospheric humidity by shallow convection preceding deep convective activity (e.g., Kemball-Cook and Weare 2001; Benedict and Randall 2007).

As another school of thought, a series of papers (Raymond 2001; Fuchs and Raymond 2002, 2005; Raymond and Fuchs 2009; Sobel and Maloney 2012,

Corresponding author address: Minoru Chikira, Research Institute for Global Change, JAMSTEC, 3173-25 Showa-machi Kanazawa-ku, Yokohama, Kanagawa 236-0001, Japan.
E-mail: chikira@jamstec.go.jp

DOI: 10.1175/JAS-D-13-038.1

2013) explored a hypothesis that the MJO can be explained as a moisture mode, which appears from a set of simplified equations and is characterized by the growth of convective activity through the amplification of moisture. The gross moist stability (GMS; Neelin and Held 1987), which was originally defined as the export of moist static energy (MSE) out of the column by a unit divergent circulation, becomes an important quantity in determining the stability of the mode. The mode occurs under the weak temperature gradient (WTG) balance (Sobel et al. 2001) in which temperature tendency and horizontal temperature gradient are negligible and its behavior can be explained primarily by a humidity variable (Sugiyama 2009a; Sobel and Maloney 2012, 2013).

These ideas remain an ongoing project in systematically explaining the various observed features of the MJO. A particularly important subject appears to be to improve our understanding on how the free-tropospheric humidity varies in the tropics. The formulation of the moisture variation in the models for the moisture mode appears to be crude and needs to be improved. Despite the efforts of the previous studies (Thayer-Calder and Randall 2009; Benedict and Randall 2007), understanding of the humidity variation in the life cycle of the MJO is still elusive. What makes it difficult is the anomalous moistening effect of the large-scale upward motion and the anomalous drying effect of the deep convection, both of which dominate in the mature phase of the MJO, mostly cancel out (e.g., Benedict and Randall 2007), resulting in small values of moisture tendency. It is not easy to understand how such small values are determined.

One existing approach to overcome this problem is to use column-integrated MSE, which is a measure of column moisture under the WTG balance. Since the subgrid-scale cumulus effect and vapor–liquid transition never change the column MSE, its governing equation is significantly simplified and provides a clear view on how the column moisture varies. This method has been adopted to understand the results of a general circulation model (GCM), the superparameterized GCM, and reanalysis data (Back and Bretherton 2006; Maloney 2009; Maloney et al. 2010; Hannah and Maloney 2011; Kiranmayi and Maloney 2011; Andersen and Kuang 2012) and provided insights on the roles of the horizontal advection, vertical advection, radiative warming anomaly, and surface flux.

However, the use of the column MSE is not satisfactory in several respects. First, according to the results of cloud-resolving models, the moist convection is more sensitive to the lower-tropospheric humidity than to the middle and upper troposphere (Tulich and Mapes 2010; Kuang 2010). The reason is considered to be larger fractional entrainment rates of cumuli there (e.g., Siebesma and Cuijpers 1995; Lin and Arakawa 1997). Thus, the lower-tropospheric humidity is considered to have a primary importance for moist convection. The use of the column MSE obscures its effect. Second, previous studies revealed that the type of convective parameterizations is the most important factor in the GCM's representation of the MJO (Slingo et al. 1996; Lin et al. 2006). But the use of the column MSE eliminates the cumulus effect and does not provide insights on how the details of the parameterizations influence the results.

The first part of this paper (Chikira and Sugiyama 2013, hereafter Part I) showed that the eastward-propagating intraseasonal oscillation represented by the Chikira–Sugiyama (CS) scheme[1] (Chikira and Sugiyama 2010) has a similar structure to the observed MJO. This study further analyzes the results focusing on the variation of the free-tropospheric humidity and proposes a novel method to understand the moisture variation. Unlike the column MSE analysis, it is possible to focus on the moisture variation at specific levels. The CS scheme is characterized by state-dependent entrainment rates and represents the sensitivity of the deep convection to the free-tropospheric humidity without any empirical suppression schemes.

Section 2 provides the experimental design and analytical method. The results are shown in section 3 and further interpreted with some manipulation of equations in section 4. Discussion is made in section 5. Finally, a summary and conclusion are presented in section 6.

2. Experimental design and analytical method

Data analyzed in this work are identical to the AGCM experiment in Chikira and Sugiyama (2010) and Part I. The AGCM is the atmospheric part of the Model for Interdisciplinary Research on Climate, version 4.1 (MIROC4.1), with the resolution of T42 and 56 levels. The model is a developing version and almost the same as MIROC5 (Watanabe et al. 2010). It is characterized by three-dimensional primitive equations in hybrid sigma–pressure (σ–p) coordinates with a spectrum and semi-Lagrangian hybrid discretization, a probability distribution function (PDF)-based prognostic cloud scheme, a two-stream k-distribution scheme for radiation with 111 channels, level 2.5 of the Mellor–Yamada turbulence scheme, an orographic gravity wave drag, the land surface model Minimal Advanced Treatments of Surface Interaction and Runoff (MATSIRO), and prognostic aerosols with direct and indirect effects. As a cumulus

[1] In a sense, the scheme can be viewed as a modification of the Arakawa–Schubert scheme (Arakawa and Schubert 1974). See the introduction of Part I for why this term is used.

parameterization, the CS scheme is used with the entrainment formulation of Gregory (2001). The integration is made for 10 years after a spinup run of 5 years with climatological sea surface temperatures (SST) and sea ice distribution.

This study mainly analyzes the composited variables. The compositing method is identical to that in Part I. To select clear events corresponding to the MJO-like waves, the anomaly of the daily-mean outgoing longwave radiation (OLR) was first taken against the climatological daily mean, which was smoothed in advance by taking 5-day running means to remove the high-frequency variation. The base points for the composites are the local minima of the anomaly that was bandpass filtered in zonal wavenumbers 1–5 and for a period of 20–100 days and then latitudinally averaged from 10°S to 10°N. Furthermore, only the events were chosen that satisfy the following conditions. The minima must be between 60°E and 150°W and propagate eastward at least 60° through which the minimum values must be less than -0.7σ, where σ is the standard deviation of the filtered anomaly. Also, the mean unfiltered anomaly over ±10° in longitude with respect to the minima during the propagation must be less than -1.2σ.

This study analyzes the slow variation of the free-tropospheric humidity accompanying the MJO-like waves whose tendency is significantly small. To guarantee the accuracy of the analyses, almost all the composited physical quantities are evaluated at each time step and their daily mean is used for the composites. As an exception, the horizontal advection terms in the pressure coordinate are evaluated every 3 h from the 3-hourly wind fields and scalar variables at pressure levels and their daily means are made by averaging them. Its accuracy was confirmed by comparing the sum of the daily-mean zonal and meridional advection terms calculated in this way with the daily-mean tendency by the dynamical process minus the vertical advection term, which were evaluated at each time step. The errors are negligible compared to the other composited tendencies. Comparison between the model and the Interim European Centre for Medium-Range Weather Forecasts (ECMWF) Re-Analysis (ERA-Interim) is made for several selected variables. The OLR provided by the Advanced Very High Resolution Radiometer (AVHRR) from 1989 to 2005 is used for the composites of the ERA-Interim dataset of the same period. In the case of the ERA-Interim dataset, the daily mean is made by averaging the 6- or 3-hourly data depending on variables.

3. Results

Figures 1a and 1b show the latitudinally averaged time–height sections of the composited moisture anomalies. Hereafter, the anomalies are the departure from the mean values from day −30 to 20 and the ranges of the latitudinal mean are 10°S–5°N and 15°S–5°N for the reanalysis and model, respectively. The model's range is determined considering that the convective center tends to be located more southward than that of the reanalysis (see section 4 of Part I). Although the model's positive moisture anomaly is overall smaller and the peak is higher compared to those of the reanalysis, the model successfully represents some basic structures such as the moister and drier free troposphere inside and to the west of the convective area, respectively. The model also exhibits the westward tilt, although it is weaker than that of the reanalysis. Since these moisture anomalies propagate eastward, the moisture tendencies show the moistening and drying to the east and west of the convective center, respectively, in both the reanalysis and model (Figs. 1c,d). The model's tendency is weaker than that in the reanalysis, reflecting that the model's MJO-like waves have the lower-frequency bias in the OLR power spectrum (Part I).

The goal of this study is to understand how these tendencies are formed. For this purpose, it is convenient to first divide the moisture tendency into the part via horizontal advection (Figs. 1e,f) and the rest (Figs. 1g,h). The latter term indicates the net effect of the vertical advection and all the physical processes. In the free troposphere, the effect of the physical processes means mostly the cloud effects, including the cumulus convection, large-scale condensation, and evaporation. The net effect of the vertical advection and the cloud processes is referred to here as the ''column process.''

The column process moistens the free troposphere below 300 hPa through all the stages of the composited waves in both the reanalysis and model. In particular, the moistening is enhanced over the convective area, suggesting that the column process works as a positive feedback to the positive moisture anomaly (see Fig. 9c for the anomalous form). This feature supports the concept of the moisture-mode theory [here, the term ''moisture mode'' is used in a broad sense that includes the column MSE instability in Kuang (2011)]. On the other hand, the horizontal advection tends to dry the free troposphere through all the stages of the waves and it is enhanced over the western margin of the convective area. In the anomaly form, it shows the moistening and drying in the eastern and western sides, respectively (Fig. 9b), which is consistent with the previous studies (e.g., Benedict and Randall 2007; Maloney 2009). The column process never shows the strong tendency for the eastward propagation, though the reanalysis shows the slightly larger moistening in the eastern side

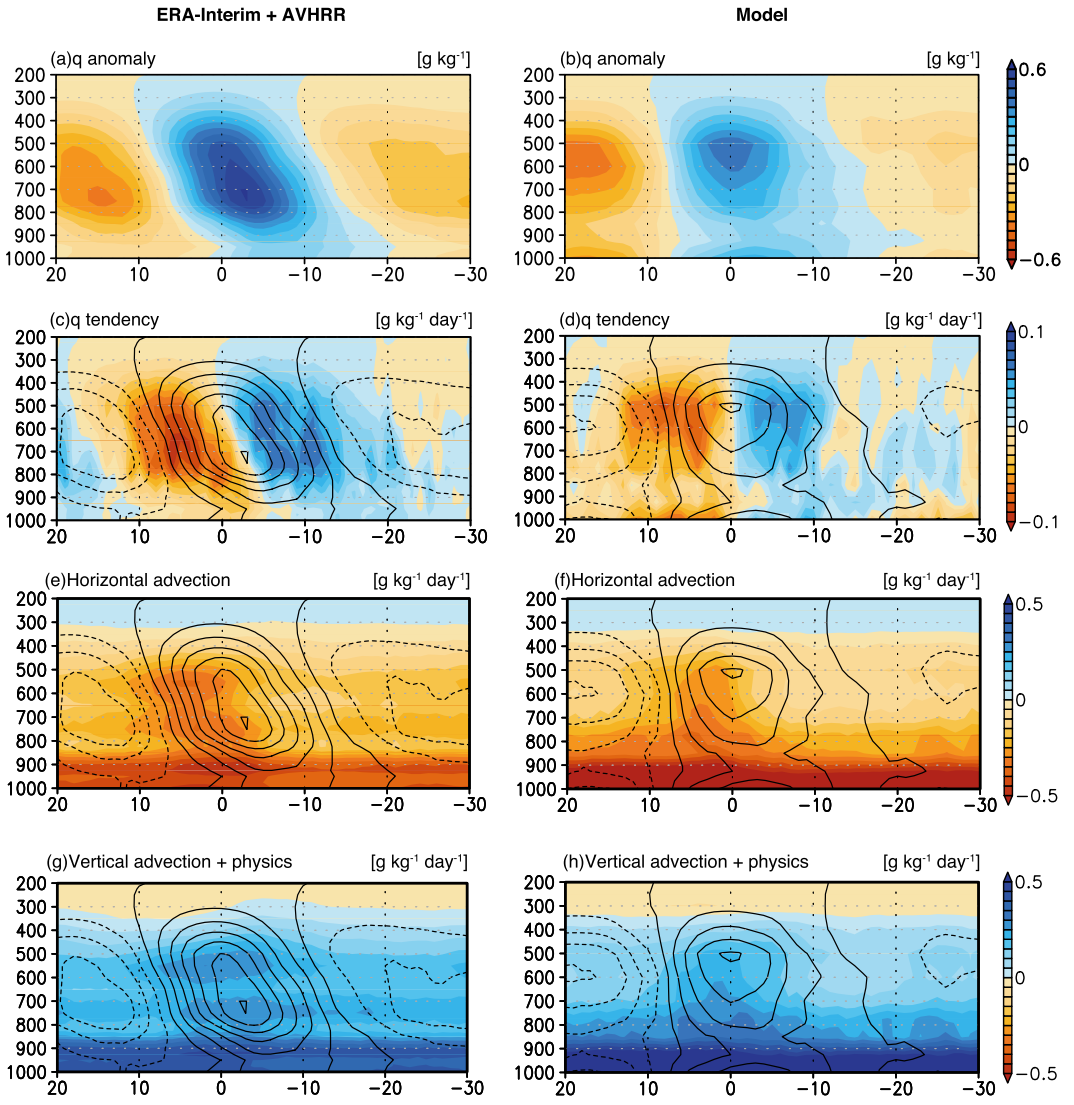

FIG. 1. Time–height sections of the composited (a),(b) anomalies, (c),(d) tendencies, and (e),(f) horizontal advection of the specific humidity. (g),(h) Tendencies of the specific humidity by the column process. (left) ERA-Interim and (right) model. Note that only (a),(b) are displayed as anomalous forms. Units are given above each panel. Contours in (c)–(h) indicate the specific humidity anomalies and the intervals are 0.1 g kg^{-1}. Unit of abscissa is days. Values in (g),(h) are calculated as the total tendency minus horizontal advection.

around 750 hPa, which presumably corresponds to the preconditioning by the shallow convection (Kemball-Cook and Weare 2001). In the case of the model, the moistening by the column process shows the slight westward shift rather than the eastward shift. Therefore, the enhanced drying to the west of the convective center by the horizontal advection causes the eastward propagation in cooperation with the amplification of the positive moisture anomalies by the column process. The drying effect of the horizontal advection is slightly weakened in the eastern margin of the convective area around days −10 and −15 in the reanalysis and model, respectively, which also contributes to the eastward propagation to some extent.

Thus, the understanding of the total moisture tendencies is divided into two parts. (1) Why does the horizontal advection particularly dry the western side of the convective area? (2) Why does the column process amplify the positive anomaly of the free-tropospheric humidity?

a. Horizontal advection

To demonstrate to what extent the high-frequency waves whose time scales are shorter than the MJO play

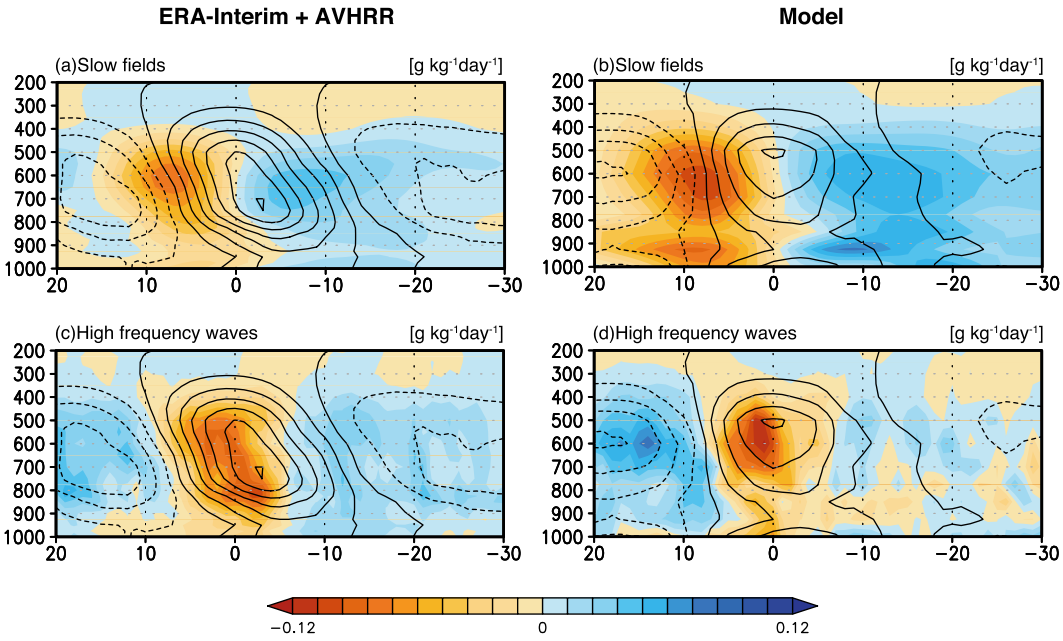

FIG. 2. Composited horizontal advection anomalies of the specific humidity (g kg^{-1} day^{-1}) by the (a),(b) slow fields and (c),(d) high-frequency waves in (left) the ERA-Interim and (right) the model. Contours indicate specific humidity anomalies with a contour interval of 0.1 g kg^{-1}. Unit of abscissa is days.

a role in the horizontal advection, the moisture advection term is decomposed as

$$-\boldsymbol{v}_h \cdot \nabla q = -\langle \boldsymbol{v}_h \rangle \cdot \nabla \langle q \rangle + F, \tag{1}$$

where

$$F \equiv -\langle \boldsymbol{v}_h \rangle \cdot \nabla q' - \boldsymbol{v}_h' \cdot \nabla \langle q \rangle - \boldsymbol{v}_h' \cdot \nabla q';$$

$\boldsymbol{v}_h$ and q denote horizontal wind and specific humidity, respectively. The angle brackets indicate the slow variation, which is composed of the Fourier components with periods more than 20 days including the mean states. The primes indicate the departures from the slowly varying fields and are composed of the Fourier components with periods less than 20 days. The first term on the right-hand side of (1) is the horizontal advection of the slowly varying moisture field by the slowly varying horizontal wind. In F, all the terms include the prime quantities, which means that F is generated by the presence of the high-frequency waves. Hereafter, the first term on the right-hand side of (1) and F are referred to simply as the horizontal advection by the slow fields and high-frequency waves, respectively.

Figure 2 shows the anomalies of the composited horizontal advection by the slow fields and high-frequency waves. The anomalous horizontal advection by the slow fields dries the western margin of the convective area in the middle troposphere and moistens the eastern side (Figs. 2a,b). The model tends to produce the greater drying in the lower troposphere than the reanalysis. The effect of the high-frequency waves tends to dry the interior of the convective area with slight westward shifts and moisten the margins of the convective area (Figs. 2c,d). Its effect appears to play a role similar to horizontal diffusion or damping, which is consistent with the observational and modeling studies by Peters et al. (2008), Maloney et al. (2010), and Andersen and Kuang (2012) and supports the idealized formulation of the eddy advection in Sobel and Neelin (2006). In the reanalysis, the drying in the western margin of the convective area is mainly caused by the zonal component of the horizontal advection by the slow fields (Figs. 3a,c), while in the model the meridional component also contributes to the drying (Figs. 3b,d). The moistening in the eastern side is primarily caused by the zonal component advection by the slow fields. The model produces the excessively enhanced drying and moistening near the boundary layer, which is presumably due to the overestimation of the negative sea level pressure anomaly (Part I). In the effect of the high-frequency waves, the zonal component contributes to the drying over the convective area more than the meridional component (Figs. 3e–h).

Figures 4a and 4b are the anomalous zonal wind velocity. The low-level anomalous convergence extends from the surface to 400 hPa, reflecting the top-heavy

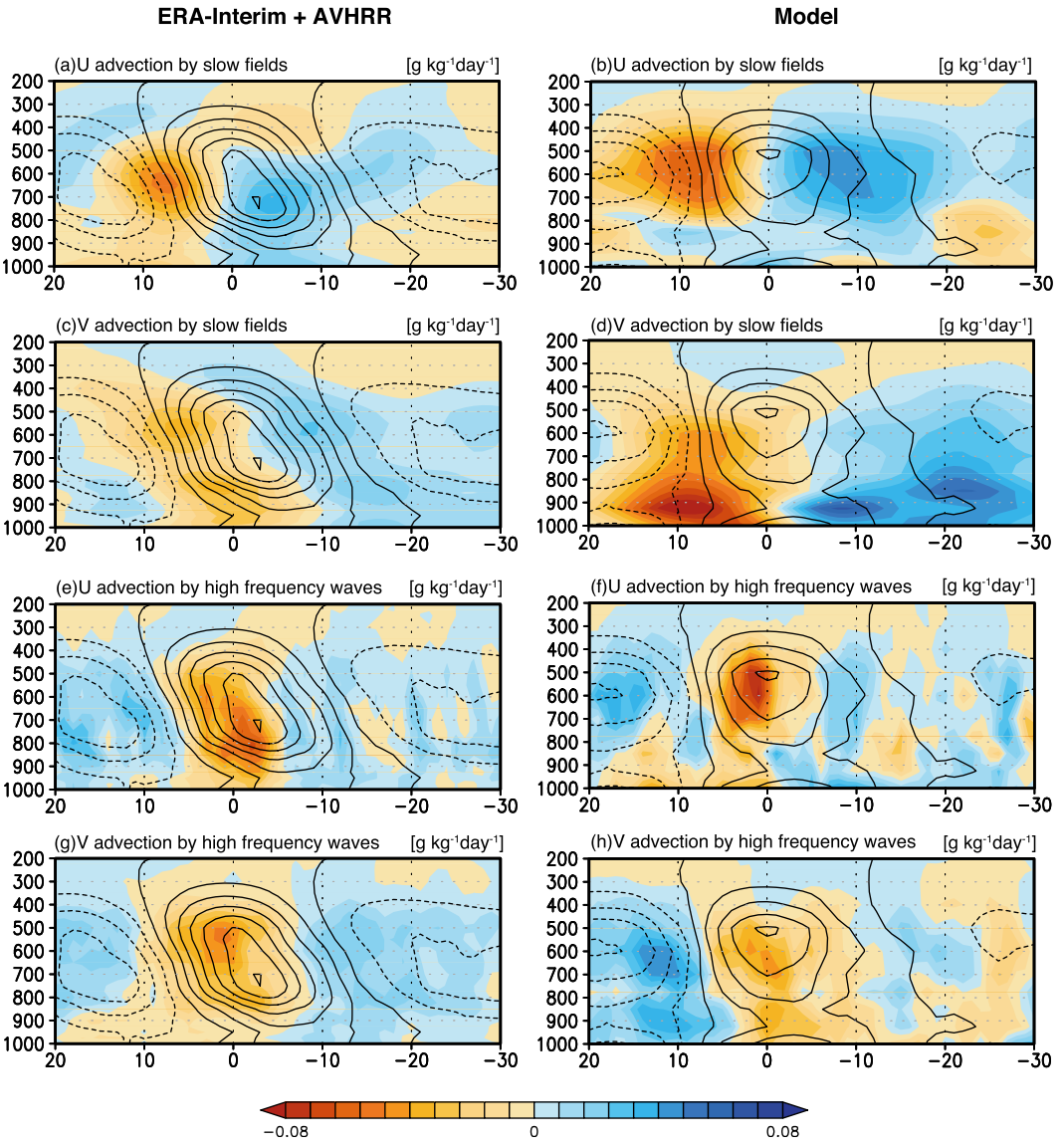

FIG. 3. Composited (a),(b) zonal and (c),(d) meridional advection anomalies of specific humidity ($g\,kg^{-1}\,day^{-1}$) by the slow fields in (left) the ERA-Interim and (right) the model. (e)–(h) As in (a)–(d), but for the advection by the high-frequency waves. Contours indicate specific humidity anomalies with a contour interval of $0.1\,g\,kg^{-1}$. Unit of abscissa is days.

heating profile (Part I). The drying over the western margin of the convective area due to the zonal component of the horizontal advection by the slow fields (Figs. 3a,b) corresponds to the westerly wind and the strong zonal gradient of the moisture there (Figs. 1a,b). In the eastern side, both the zonal moisture gradient and wind velocity are weaker than those in the western side, which explains the anomalous moistening by the zonal component advection of the slow fields there. The horizontal wind anomaly at 800 hPa in the model shows a clear Rossby wave response to the convective heating around 15°S and day 0, which transports the dry air from the extratropics to the western part of the convective region (Fig. 4d). Since the convective center is shifted southward, the Rossby wave response is predominant to the south of the equator. A qualitatively similar but weaker response is seen at 600 hPa as well around 10°S and day 0 (Fig. 4f). At 200 hPa, the direction of the anomalous wind becomes opposite and a counterclockwise circulation is seen to the south of the equator around day 0 (Fig. 4h). The qualitatively same response is seen in the reanalysis as well, but the Rossby wave gyres are more obscured (Figs. 4c,e,g). The model's greater Rossby wave response is considered to be related to the excessively

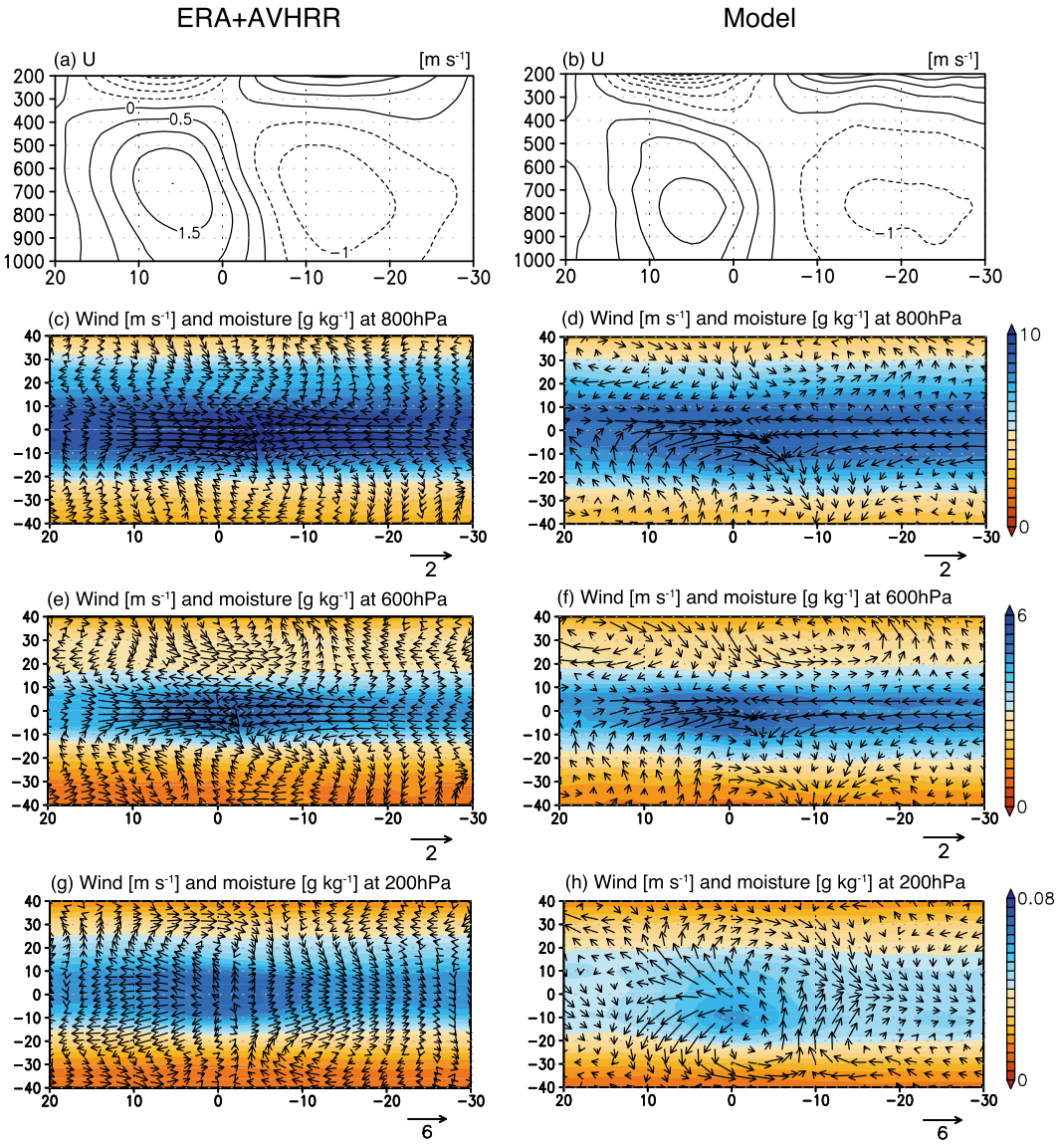

FIG. 4. (a),(b) Anomalies of the composited zonal wind velocity. Specific humidity (shading) and horizontal wind (vectors) anomalies at (c),(d) 800, (e),(f) 600, and (g),(h) 200 hPa. (left) Reanalysis and (right) model. Units are shown above each panel. Unit of abscissa is days. Ordinate in (c)–(h) is latitude (°).

low sea level pressure over the convective area (Part I) and is responsible for the larger drying due to the meridional component of the horizontal advection by the slow fields (Fig. 3d). The Rossby wave circulation explains the drying by the meridional component of the slow field advection. Even in the eastern side of the convective area, the Rossby wave generates slightly poleward circulation in the lower and middle troposphere and contributes to the moistening there. The importance of the Rossby wave circulation in drying the western side through dry air advection from the extratropics was discussed in previous studies using reanalysis data (Maloney and Hartmann 1998) and a simplified model (Sugiyama 2009b). The result of this study supports them.

b. *Column process*

To examine how the column process amplifies the positive free-tropospheric moisture anomaly, the budget analysis of the free-tropospheric moisture is made. The prognostic equation of the free-tropospheric specific humidity in the pressure coordinate is given by

$$\frac{\partial q}{\partial t} = -\boldsymbol{v}_h \cdot \nabla q - \omega \frac{\partial q}{\partial p} + S_{\mathrm{cu}} - \tilde{C} + \tilde{R}_v + S_{\mathrm{df}}, \qquad (2)$$

where the tildes denote the mean values in the surrounding environment outside of cumuli in a grid. The quantities without the tildes are grid-mean values. On the right-hand side, S_{cu} and S_{df} are source terms by subgrid-scale moisture transport by cumulus ensemble and vertical diffusion, respectively; C is the large-scale condensation of water vapor minus evaporation of cloud water; and R_v is the reevaporation of precipitation. The other symbols follow the standard notation.

In the middle and lower troposphere over the convective area of the MJO, the absolute values of the anomalous vertical advection and cumulus term are much larger than those of the other terms and these two terms mostly cancel out, resulting in much smaller values, which makes it difficult to understand why such small values remain. To overcome this problem, the cumulus term is decomposed into the effects of detrainment and subsidence as

$$S_{cu} = D_q - \omega_c \frac{\partial q}{\partial p}, \tag{3}$$

where D_q and ω_c denote the moisture tendency by the detrainment and the vertical velocity due to the cumulus subsidence, respectively. The reevaporation of cumulus precipitation also exists and is included in R_v in (2). The term of cumulus downdraft detrainment is omitted since it affects only near boundary layer as shown later. Note that the effect of the downdraft mass flux on environmental vertical motion is included in ω_c. Equations (2) and (3) lead to

$$\frac{\partial q}{\partial t} = -\boldsymbol{v}_h \cdot \nabla q - \tilde{\omega}\frac{\partial q}{\partial p} + D_q - \tilde{C} + \tilde{R}_v + S_{df}, \tag{4}$$

where $\tilde{\omega} = \omega + \omega_c$ is referred to as environmental vertical velocity. Since the anomalies of the second terms on the right-hand side of (2) and (3) mostly cancel out in the middle and lower troposphere in the mature phase of the model's MJO-like waves, the anomaly of the second term on the right-hand side of (4) (environmental vertical advection) becomes much smaller and comparable to the other terms (shown later).

Next, the prognostic equation of potential temperature in the free troposphere is given by

$$\frac{\partial \theta}{\partial t} + \boldsymbol{v}_h \cdot \nabla\theta + \omega\frac{\partial \theta}{\partial p} = \frac{1}{C_p \pi}[Q_{cu} + L_v(\tilde{C} - \tilde{R}_v) + Q_r + \tilde{Q}_i + Q_{df}], \tag{5}$$

where θ, π, C_p, and L_v denote potential temperature, the Exner function, specific heat at constant pressure, and latent heat of vaporization, respectively. The terms Q_{cu}, Q_i, Q_r, and Q_{df} are heating by the subgrid-scale cumulus effect, liquid–ice transition, radiation, and vertical diffusion, respectively. Note that with regard to sublimation, the heat corresponding to the vapor–liquid transition is included in L_vC and L_vR_v and that corresponding to the liquid–ice transition is Q_i.

Applying the WTG approximation (Sobel et al. 2001), the first and second terms in the left-hand side of (5) are neglected. In addition, the cumulus effect is again decomposed into the effects of the detrainment and subsidence as

$$\frac{Q_{cu}}{C_p \pi} = D_\theta - \omega_c \frac{\partial \theta}{\partial p}, \tag{6}$$

where D_θ is θ tendency by the cumulus detrainment. For the sublimation of the cumulus precipitation, the heat corresponding to the liquid–vapor transition is included in L_vR_v and that corresponding to the liquid–ice transition is Q_i. The term of the downdraft detrainment is omitted. Equations (5) and (6) with the WTG approximation lead to

$$\tilde{\omega}\frac{\partial \theta}{\partial p} = D_\theta + \frac{1}{C_p \pi}[L_v(\tilde{C} - \tilde{R}_v) + Q_r + \tilde{Q}_i + Q_{df}]. \tag{7}$$

This equation shows a thermodynamic balance that regulates $\tilde{\omega}$. The effect of the high-frequency waves in the left-hand side of (7) is much smaller on average than that of slow fields, as shown later. The $\tilde{\omega}$ determined by this balance influences the moisture tendency through the second term on the right-hand side of (4).

Hereafter, only the model results are shown. Figure 5a shows the time-mean profiles of the θ tendencies due to each of the terms. The time-mean $\tilde{\omega}$ profile is also shown in Fig. 5c. Since ω_c is necessary to calculate $\tilde{\omega}$, it is estimated from the mass flux of the cumulus subsidence assuming $\omega \simeq -\rho g w$, where ρ, g, and w are density, gravity, and vertical velocity in the z coordinate.

The total tendency and horizontal advection effect are negligible compared to the other terms. The effect of the downdraft detrainment is important only near the surface. In the upper troposphere, the cooling by the radiation is larger than the heating by $\tilde{C}$, which causes the weak downward $\tilde{\omega}$. In the lower troposphere, the net cooling effect by the radiation and evaporation (both cloud and precipitation) causes the strong cooling and is balanced by the heating due to the downward $\tilde{\omega}$. In the middle troposphere, the cooling by the radiation, liquid–ice transition, and $\tilde{C}$ is balanced by the heating effect of the downward $\tilde{\omega}$. The cooling by the liquid–ice transition is mostly caused by the melting of snow (not shown).

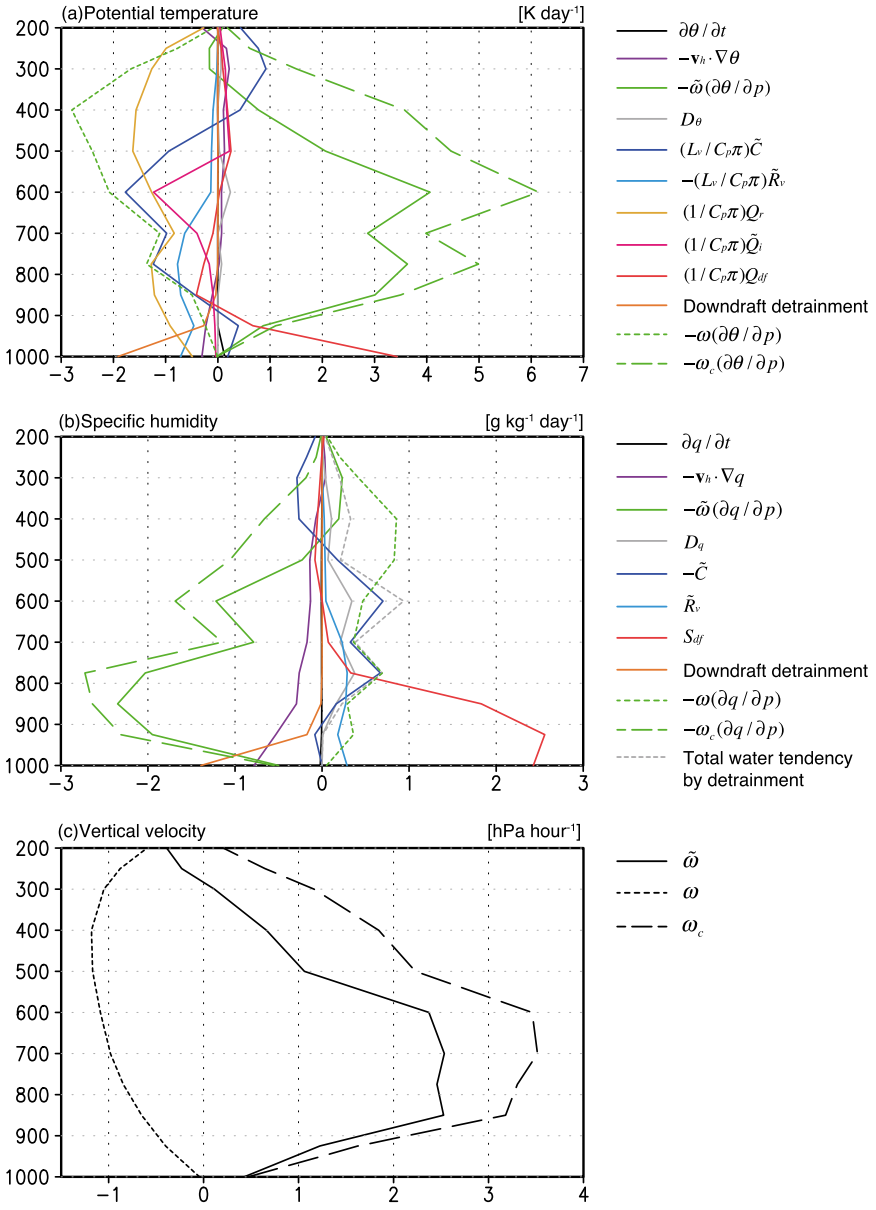

FIG. 5. Composited (a) potential temperature and (b) specific humidity tendencies by each of the terms in (7) and (4) averaged from days −30 to 20 (solid lines). Total tendency and tendencies by horizontal advection and downdraft detrainment are also shown. Corresponding line colors are shown to the right of the panels. Short- and long-dashed green lines in (a) and (b) indicate the tendencies of the vertical advection terms by ω and ω_c, respectively. In (b), total water tendency by the detrainment is shown by a gray dashed line. (c) Environmental (solid), mean (short dashed), and cumulus subsidence (long dashed) vertical velocity averaged from days −30 to 20. Units are shown above each panel.

The effect of the detrainment is very small. Note that $\tilde{\omega}$ is downward in the whole troposphere, except for near the tropopause.

The mean moisture tendencies by each of the terms in (4) are shown in Fig. 5b. The effect of the downdraft detrainment is important only near the surface. In the lower free troposphere, the moistening by the vertical diffusion, reevaporation of the precipitation, $\tilde{C}$, and detrainment is balanced by the drying effects of the downward environmental vertical and horizontal advection. The vertical diffusion scheme adopted in this model is based on a moist closure and can represent

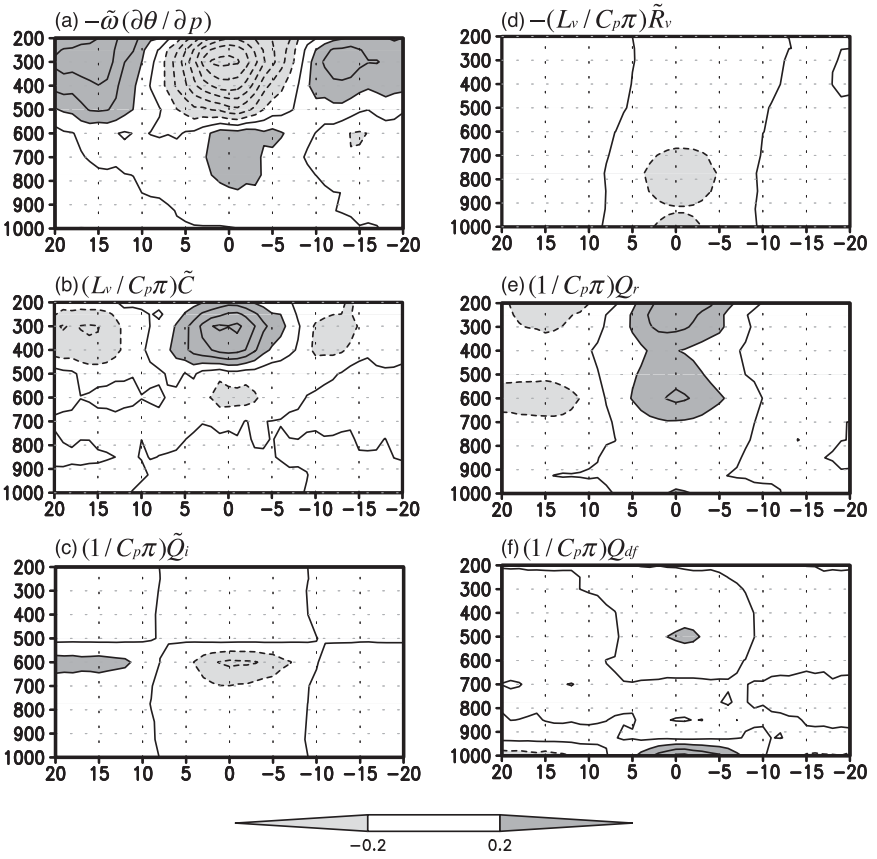

FIG. 6. Composited potential temperature tendency anomalies by each of the terms in (7). Contour interval is 0.2 K day^{-1}. Unit of abscissa is days.

shallow convection (hereafter, the term ''shallow convection'' is used to indicate moist convection that detrains around 850 hPa) to some extent. The moistening by the vertical diffusion above 900 hPa is considered to be due to shallow convection represented by the scheme. In the middle troposphere, the moistening by the reevaporation, $\tilde{C}$, and detrainment is balanced by the drying effect of the downward environmental vertical advection. In the upper troposphere, the moistening by the environmental vertical advection is balanced by the removal of the moisture owing to $\tilde{C}$. Figure 5c shows that the mean $\tilde{\omega}$ is weakly downward between 300 and 400 hPa, but its advection works as moistening, which is considered to be due to the eddy moisture transport. Figure 5b also shows the total water tendency by the detrainment. It is approximately 3 times as large as the moisture tendency in the middle and upper troposphere, which exhibits that the large part of water is transported upward in the form of liquid and ice water. There are two positive peaks of $\tilde{C}$ (at 600 and 775 hPa), which correspond to those of the total water tendency by the detrainment, suggesting that the large part of the detraining cloud water evaporates there.

Figure 6 shows the time–height sections of the θ tendency anomalies by each of the terms in (7). The total tendency, the effect of the horizontal advection, and that of the detrainment are omitted because their absolute values are smaller than 0.2 K day^{-1} everywhere. The tendency by the downdraft detrainment is also omitted, because it is important only near the surface and its values are smaller than 0.2 K day^{-1} in the entire free troposphere. The time–height section of $\tilde{\omega}$ anomaly is given in Fig. 7. Overall, the time–height structures are symmetrical with respect to day 0. The profiles averaged from day −5 to 5 are shown in Fig. 8a for θ tendencies and Fig. 8c for $\tilde{\omega}$. In the upper troposphere, the heating by $\tilde{C}$ is a dominant factor in causing the large upward environmental vertical velocity anomaly. The radiative heating anomaly secondarily contributes to it. In the lower troposphere, the cooling by the reevaporation of the precipitation overcomes the radiative warming anomaly, thereby causing the weak downward $\tilde{\omega}$ anomaly. In the middle troposphere, the cooling by $\tilde{C}$ and the liquid–ice transition mostly caused by the increased melting of snow (not shown) contributes to the downward $\tilde{\omega}$ anomaly there. While the mean $\tilde{\omega}$ and ω_c have

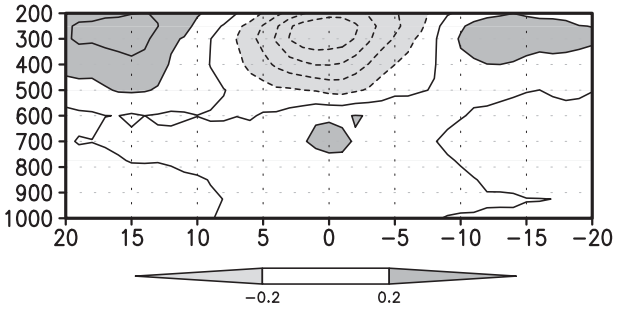

FIG. 7. Composited environmental vertical velocity anomaly. The contour interval is 0.2 hPa h^{-1}. Unit of abscissa is days.

similar profiles (Fig. 5c), the anomaly of $\tilde{\omega}$ is very different from that of ω_c. It has much smaller values in the lower troposphere, since ω and ω_c mostly cancel out there. The same applies to the mean and anomalous θ tendencies by $\tilde{\omega}$ and ω_c.

Figure 9 shows the time–height sections of the moisture tendency anomalies by each of the terms in (4). As is already seen, the total and horizontal advection tendencies have asymmetrical structures with respect to day 0. Compared to them, the rest of the terms are generally symmetrical, so it is convenient to see the profiles averaged from day −5 to 5 (Fig. 8b) in order to examine them quantitatively. In the upper troposphere, there is a large moistening by the upward $\tilde{\omega}$ anomaly. Most of it is canceled out by $-\tilde{C}$ and the small positive tendency of the column process remains. In the lower troposphere, the moistening by the reevaporation of the precipitation overcomes the drying by the downward $\tilde{\omega}$ anomaly, resulting in the small positive tendency of the column process. In the middle troposphere, the evaporation of the cloud water is a dominant moistening factor. The effect of the detrainment is very small in the entire free troposphere, but the total water tendency by the detrainment (gray dashed line in Fig. 8b; see also Fig. 10a for the time–height section) is much larger than the moisture counterpart, exhibiting the increased transport of the water by the cumuli is made in the form of cloud water. The large moistening anomaly by $-\tilde{C}$ at 600 hPa corresponds to the peak anomalous tendency of the total water by the detrainment, suggesting that the large part of the increased detraining cloud water evaporates there, which does contribute to the moistening of the middle troposphere. The downdraft detrainment is important only near the surface. The effect of the vertical diffusion shows large values near the surface. It also shows a small amount of drying around 500 hPa, which is presumably caused by the enhanced mixing owing to the radiative cooling at the upper surface of the clouds in the middle troposphere. The absolute values of the moisture tendencies by the ω and ω_c advection (short- and long-dashed green lines in Fig. 8b) are much larger than the other terms in the middle and lower troposphere, but they mostly cancel out and the $\tilde{\omega}$ advection tendency becomes comparable to the other terms there. The detrainment mass flux anomaly (Fig. 10b) shows its enhancement in the upper and middle troposphere; thus, both the deep convection and congestus clouds are enhanced in the mature phase of the MJO-like waves.

4. Further interpretation on column process

To further illuminate how the slow variation of the free-tropospheric moisture is controlled, this section discusses an equation controlling slowly varying specific humidity by combining (4) and (7).

First, the environmental vertical advection terms for θ and q are divided into two terms by substituting $\theta = \langle\theta\rangle + \theta'$, $q = \langle q\rangle + q'$, and $\tilde{\omega} = \langle\tilde{\omega}\rangle + (\tilde{\omega})'$:

$$-\tilde{\omega}\frac{\partial\theta}{\partial p} = -\langle\tilde{\omega}\rangle\frac{\partial\langle\theta\rangle}{\partial p} + Q_{\rm hf} \quad \text{and} \tag{8}$$

$$-\tilde{\omega}\frac{\partial q}{\partial p} = -\langle\tilde{\omega}\rangle\frac{\partial\langle q\rangle}{\partial p} + S_{\rm hf}, \tag{9}$$

where

$$Q_{\rm hf} = -\langle\tilde{\omega}\rangle\frac{\partial\theta'}{\partial p} - (\tilde{\omega})'\frac{\partial\langle\theta\rangle}{\partial p} - (\tilde{\omega})'\frac{\partial\theta'}{\partial p} \quad \text{and}$$

$$S_{\rm hf} = -\langle\tilde{\omega}\rangle\frac{\partial q'}{\partial p} - (\tilde{\omega})'\frac{\partial\langle q\rangle}{\partial p} - (\tilde{\omega})'\frac{\partial q'}{\partial p}.$$

The terms $Q_{\rm hf}$ and $S_{\rm hf}$ are generated by the presence of the high-frequency waves. Figure 11 shows the composited $Q_{\rm hf}$ and $S_{\rm hf}$ anomalies. Compared to the total environmental vertical advection terms in Figs. 6a and 9d, these terms are generally small. Note that $Q_{\rm hf}$ is negligible compared to $\tilde{\omega}\partial\theta/\partial p$ between days −5 and 5. The time-mean value of $Q_{\rm hf}$ is negligible compared to that of the second term on the right-hand side of (8) (not shown). Thus, the approximation

$$\tilde{\omega}\frac{\partial\theta}{\partial p} \simeq \langle\tilde{\omega}\rangle\frac{\partial\langle\theta\rangle}{\partial p} \tag{10}$$

holds in the composited fields. Although $S_{\rm hf}$ is relatively small, it is not negligible compared to the other terms in (4). Using (10) in (7) and omitting the cumulus detrainment term,

$$\langle\tilde{\omega}\rangle\frac{\partial\langle\theta\rangle}{\partial p} \simeq \frac{1}{C_p\pi}[L_v(\tilde{C} - \tilde{R}_v) + Q_r + \tilde{Q}_i + Q_{\rm df}] \tag{11}$$

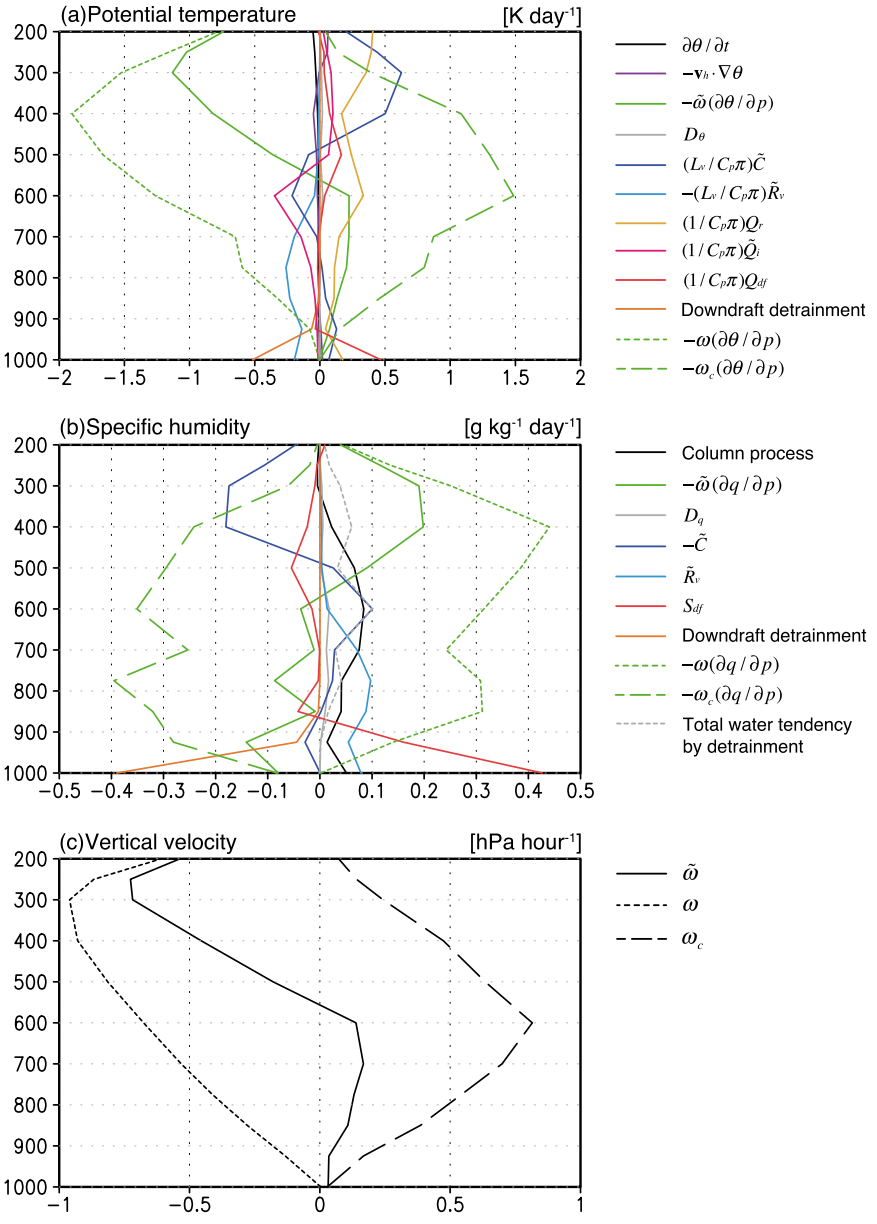

FIG. 8. As in Fig. 5, but for anomalies averaged from days −5 to 5. Note that black line in (b) indicates the specific humidity tendency by the column process instead of the total.

is obtained. Note that this equation holds only when the MJO-composited values are substituted into each of the terms on the left- and right-hand sides. Dividing (11) by $\partial\langle\theta\rangle/\partial p$, one obtains

$$\langle\tilde{\omega}\rangle \simeq \frac{1}{C_p\pi}[L_v(\tilde{C}-\tilde{R}_v)+Q_r+\tilde{Q}_i+Q_{\rm df}]\left(\frac{\partial\langle\theta\rangle}{\partial p}\right)^{-1}. \tag{12}$$

Using (9) in (4) and eliminating $\langle\tilde{\omega}\rangle$ by (12), the q tendency by the column process is given by

$$\left(\frac{\partial q}{\partial t}\right)_{\rm col} \simeq (\alpha-1)(\tilde{C}-\tilde{R}_v)+\frac{\alpha}{L_v}(Q_r+\tilde{Q}_i+Q_{\rm df}) + D_q+S_{\rm df}+S_{\rm hf}, \tag{13}$$

where the subscript "col" indicates the column process. The nondimensional parameter α is written as

$$\alpha \equiv -\frac{L_v}{C_p\pi}\left(\frac{\partial\langle q\rangle}{\partial p}\right)\left(\frac{\partial\langle\theta\rangle}{\partial p}\right)^{-1}, \tag{14}$$

and generally has positive values. After some manipulation using hydrostatic balance, α can also be written as

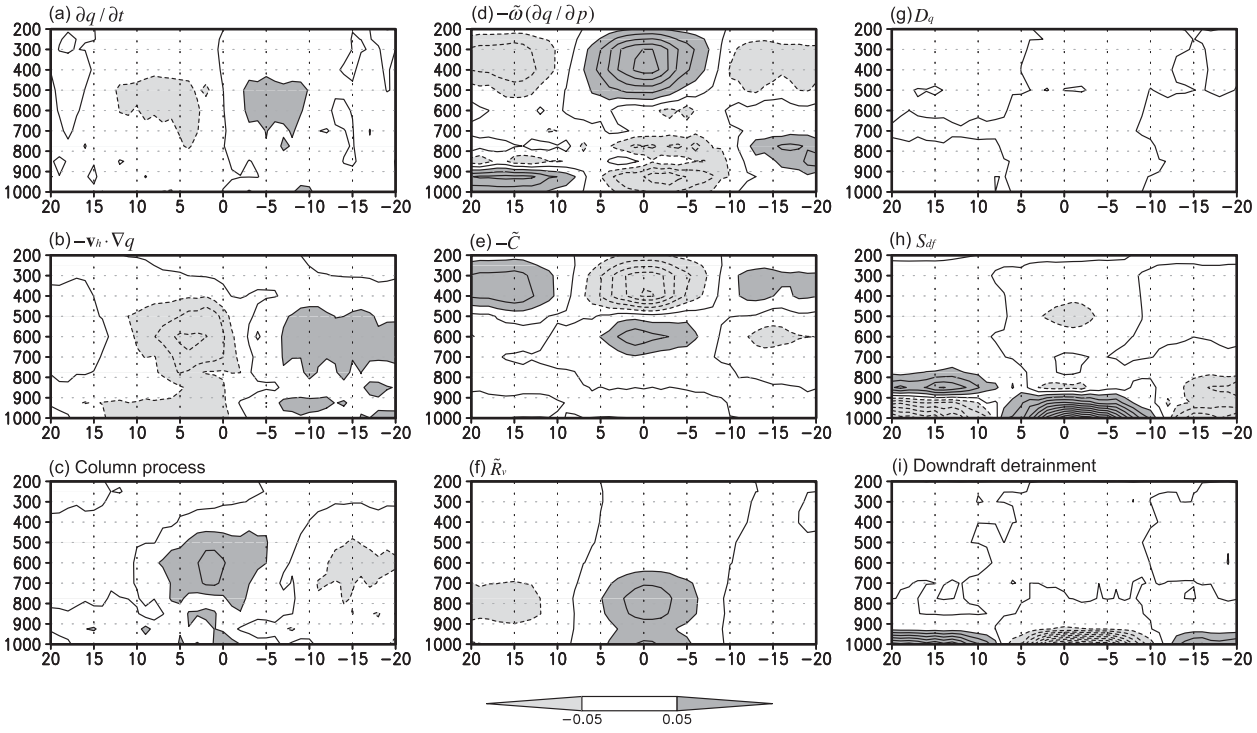

FIG. 9. Composited specific humidity tendency anomalies by each of the terms in (4). Contour intervals are $0.06\,\mathrm{g\,kg^{-1}\,day^{-1}}$.

$$\alpha \equiv -L_v\left(\frac{\partial\langle q\rangle}{\partial z}\right)\left(\frac{\partial\langle s\rangle}{\partial z}\right)^{-1}, \tag{15}$$

where s is dry static energy. Although it is not necessarily guaranteed any more that (13) holds when the composited values are substituted into each of the terms, it should hold for the typical slow life cycle of the MJO-like waves.

In (13), the terms with α represent their effects through the environmental vertical advection. The second term on the right-hand side of (13) shows that heating (cooling) by radiation, liquid–ice transition, and vertical diffusion leads to upward (downward) $\tilde{\omega}$ and moistens (dries) the atmosphere. The first term on the right-hand side of (13) shows that the large-scale condensation (evaporation) works as a drying (moistening) factor (the term with -1), but at the same time, it warms (cools) the atmosphere and causes upward (downward) $\tilde{\omega}$, which works as a moistening (drying) factor (the term with α). Here α characterizes the efficiency of moistening (drying) through upward (downward) environmental vertical velocity generated by external heating (cooling). In (14), $\partial\langle\theta\rangle/\partial p^{-1}$ represents the effect of the static stability on $\langle\tilde{\omega}\rangle$ through (12). Larger (smaller) static stability reduces (enhances) the absolute values of $\langle\tilde{\omega}\rangle$, given the same amount of external heating or cooling. Also in (14), $\partial\langle q\rangle/\partial p$ represents the factor with which $\langle\tilde{\omega}\rangle$ affects the moisture tendency through $-\langle\tilde{\omega}\rangle\partial\langle q\rangle/\partial p$. Larger (smaller) $\partial\langle q\rangle/\partial p$ enhances (reduces) either the moistening or drying effect by the upward or downward environmental vertical advection, respectively, given the same values of $\langle\tilde{\omega}\rangle$. The

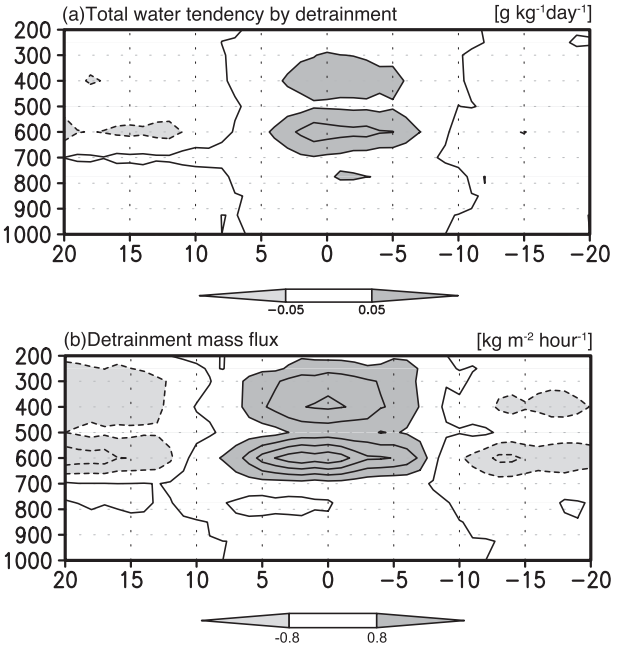

FIG. 10. Composited (a) total water tendency by detrainment and (b) detrainment mass flux anomalies. Contour intervals are (a) $0.05\,\mathrm{g\,kg^{-1}\,day^{-1}}$ and (b) $0.8\,\mathrm{kg\,m^{-2}\,h^{-1}}$.

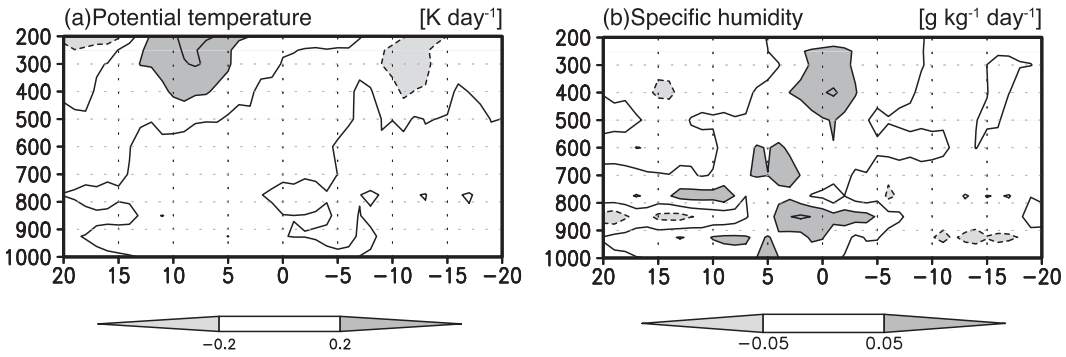

FIG. 11. The composited (a) $Q_{\rm hf}$ and (b) $S_{\rm hf}$ anomalies. See text for definitions. The units and scales for (a) and (b) are as in Figs. 6 and 9, respectively.

parameter α will be useful when considering how given profiles of temperature and moisture affect the moisture tendency under the WTG balance.

Figure 12a shows the composited α averaged between days −30 and 20 in the model and ERA-Interim, which is calculated using the composited $\tilde{q}$ and $\tilde{\theta}$. In the lower troposphere, α is large since $\partial q/\partial z$ is large there (discussed later in detail), which means that the moistening (drying) effect of the external heating (cooling) is amplified in the lower troposphere. Note that α approaches zero with increasing height, since $\partial q/\partial z$ becomes smaller. Thus, the moistening (drying) effect of the external heating (cooling) is weak in the upper troposphere.

Depending on the sign of $\alpha - 1$, the total effects of $\tilde{C}$ and $\tilde{R}_v$ are either moistening or drying. From (15),

$$\alpha - 1 = -\left(\frac{\partial\langle h\rangle}{\partial z}\right)\left(\frac{\partial\langle s\rangle}{\partial z}\right)^{-1}, \tag{16}$$

where h is moist static energy. Since $\partial\langle s\rangle/\partial z$ is always positive, the sign of $\alpha - 1$ is determined solely by that of $-\partial\langle h\rangle/\partial z$. Figure 12a shows that α is larger (smaller) than 1 below (above) 700 hPa; hence, $\alpha - 1$ is positive (negative) below (above) 700 hPa. Thus, the large-scale condensation above (below) 700 hPa works as drying (moistening), while the large-scale evaporation including both the cloud water and precipitation above (below) 700 hPa works as moistening (drying).

The drying effect of the reevaporation in the lower troposphere might seem to be inconsistent with the previous modeling studies where the increased reevaporation rate leads to the enhanced intraseasonal variability

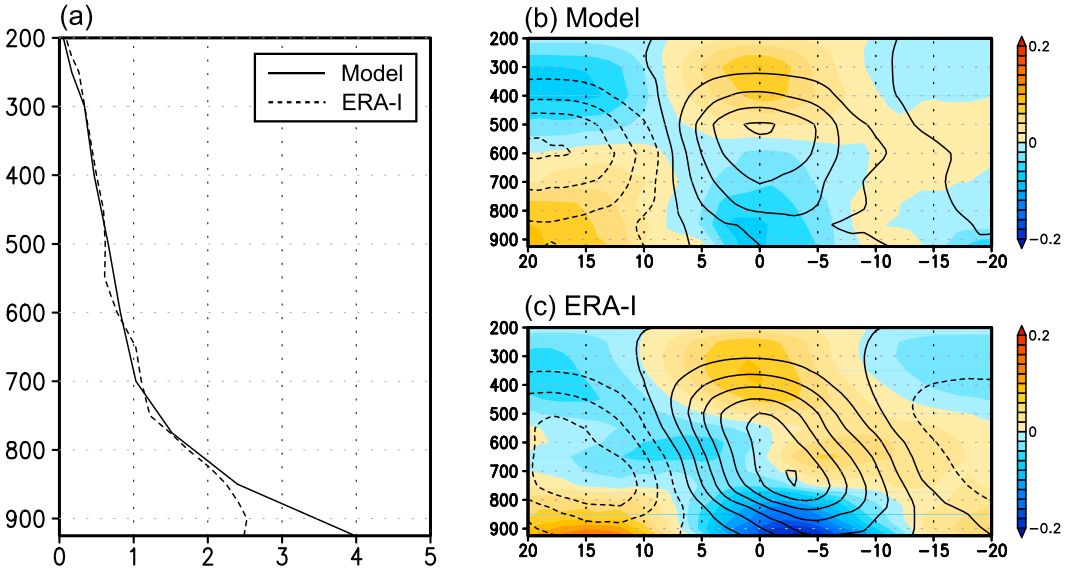

FIG. 12. (a) Vertical profile of α averaged between days −30 and 20 in the model (solid line) and ERA-Interim (dashed line). Also time–height sections of α anomalies in (b) the model and (c) the ERA-Interim. Contours indicate the specific humidity anomalies (interval is 0.1 g kg^{-1}). The composited $\tilde{q}$ and $\tilde{\theta}$ are used to calculate α.

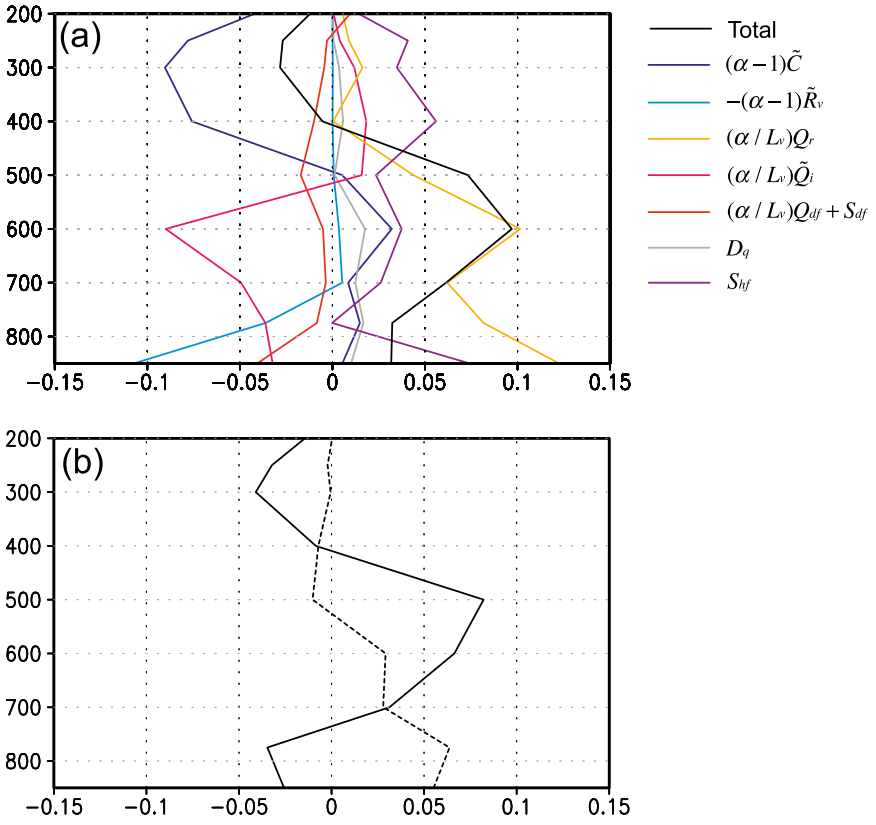

FIG. 13. (a) Anomalous specific humidity tendencies by each of the terms in (13) averaged between days −5 and 5. (b) Anomalous specific humidity tendencies by the first (solid) and second (dashed) terms in (17) averaged between days −5 and 5. Units are grams per kilogram per day.

(Maloney and Hartmann 2001; Grabowski and Moncrieff 2004; Maloney 2009; Kim et al. 2012). However, since both Maloney and Hartmann (2001) and Grabowski and Moncrieff (2004) suggested that the enhancement of the intraseasonal variability was caused by the change in the mean state of the moisture, not by the variation, this result may not contradict with theirs.

Although the heating by the condensation in the stratiform clouds induces upward motion that moistens the upper troposphere, a drying effect through the removal of the moisture is greater. It means that the heating by the stratiform clouds in the decay phase of the MJO cannot explain the positive moisture anomaly there.

As an alternative to (13), it is possible to use moist static energy instead of the moisture, since it becomes an indicator of moisture under the WTG balance. The resultant view is quite similar to (13). See appendix for details.

Figure 13a shows the moisture tendencies for each of the terms in (13) averaged over the convective area, which are calculated by using the composited values for $\tilde{C}$, $\widetilde{R_v}$, Q_r, $\widetilde{Q_i}$, Q_{df}, D_q, S_{df}, S_{hf}, and α calculated using the composited $\tilde{q}$ and $\tilde{\theta}$. The total tendency (black line) is the sum of the terms in the right-hand side of (13), which is qualitatively similar to the composited moisture tendency by the column process shown in Fig. 8b (black line).

The primary contributor to the moistening in the middle and lower troposphere is the radiative warming anomaly. While its effect on the potential temperature is small in the lower troposphere (Fig. 8a), the effect on the moisture is significantly amplified because of the large α there. The importance of the radiative warming anomaly for moistening free troposphere was discussed in the previous studies (e.g., Raymond 2001) and this result supports it. However, it should be noted that since the intraseasonal OLR variance in this model is overestimated compared to a satellite observation (Part I), the estimated effect of the radiative warming anomaly might be also exaggerated. The high-frequency waves moisten the entire free troposphere and are a primary moistening factor in the upper troposphere. Note that $\tilde{C}$ significantly dries the upper troposphere and weakly moistens the middle counterpart. Its absolute values are smaller than those in Fig. 8b above 700 hPa because they

are reduced by the term with α. The cooling by the liquid–ice transition significantly dries the middle and lower troposphere. Again, while its effect on the potential temperature is small in the lower troposphere (Fig. 8a), that on the moisture is greatly amplified by the large values of α. The reevaporation is a primary drying factor in the lower troposphere owing to the downward environmental vertical advection and large α. The cumulus detrainment plays a minor role in moistening the free troposphere. Although the positive anomaly of $(\alpha/L_v)Q_{\rm df}$ slightly moistens the free troposphere (not shown), the negative anomaly of $S_{\rm df}$ overcomes and the total effect of the vertical diffusion is drying in the entire free troposphere.

Linearizing (13) with respect to the time mean,

$$\left(\frac{\partial q'}{\partial t}\right)_{\rm col} \simeq \left\{(\overline{\alpha}-1)[(\tilde{C})'-(\tilde{R}_v)']+\frac{\overline{\alpha}}{L_v}(Q'_r+(\tilde{Q}_i)'+Q'_{\rm df}) + D'_q+S'_{\rm df}+S'_{\rm hf}\right\}+\frac{\alpha'}{L_v}[L_v(\overline{\tilde{C}}-\overline{\tilde{R}}_v) + \overline{Q}_r+\overline{\tilde{Q}}_i+\overline{Q}_{\rm df}] \tag{17}$$

is obtained, where the bar indicates the time mean and the prime is redefined as a departure from the time mean. This equation shows that the contributors to the moisture tendency are not only the terms with primes in the first term of the right-hand side but also the change in α. Figures 12b and 12c show α' in the model and ERA-Interim as departures from the time mean between days −30 and 20. In both of model and ERA-Interim, α' is negative in the lower troposphere over the convective area. In the case of the reanalysis, α' begins to become negative earlier. Since $L_v(\overline{\tilde{C}}-\overline{\tilde{R}}_v)+\overline{Q}_r+\overline{\tilde{Q}}_i+\overline{Q}_{\rm df}$ is negative in almost the entire free troposphere (Fig. 5a), the negative α' leads to the enhancement of moistening. This anomalous moistening occurs through the reduction of the drying by the downward $\tilde{\omega}$ advection under the decreased α.

Figure 13b shows the anomalous moisture tendencies by the first and second terms in (17). The first term contributes to the moistening in the middle troposphere, but it does not in the lower counterpart. The second term is the main contributor to the moistening of the lower troposphere. Lower-tropospheric humidity is much more important for the persistence of deep convective activity than the midtropospheric counterpart, since entrainment rates are greater there. Thus, the decrease in α is the direct contributor to the maintenance of the convective activity in the mature phase of the MJO-like waves. The model substantially underestimates the reduction of α compared to the reanalysis.

However, what is important for the reduction of α in the lower troposphere is the moistening of the middle troposphere and it is made by the first term in (17). As shown in Fig. 13a, the primary contributor to the midtropospheric moistening is the radiative warming anomaly. In addition, since the melting of snow substantially dries the middle troposphere, another important factor in moistening the middle troposphere is considered to be the reduction of the snow melting. This fact suggests that a larger population of deep convection is an unfavorable condition for the moistening of the free troposphere, since it results in more precipitation falling from the upper troposphere and thereby more snow melting in the middle troposphere. On the other hand, a larger population of congestus clouds and a smaller population of deep convection weaken the drying by the snow melting and lead to enhanced moistening, given the same amount of column-integrated cumulus heating. One of the unique features in the CS scheme is an increased population of congestus clouds (Chikira 2010) in climatology. Besides, Fig. 10b shows the significantly enhanced detrainment of the congestus clouds in the mature phase of the MJO-like waves. This feature is considered to play an important role in moistening the middle troposphere.

To demonstrate the importance of the lower-tropospheric heating as discussed above, a bottom-heavy heating index (BI) is defined as

$$\mathrm{BI}=\int_{600\mathrm{hPa}}^{850\mathrm{hPa}} Q_{\rm cu}\,dp \Big/ \int_{100\mathrm{hPa}}^{850\mathrm{hPa}} Q_{\rm cu}\,dp.$$

Then the heating by the liquid–ice transition, radiation, and reevaporation of the precipitation normalized by the vertical-mean cumulus heating between 100 and 850 hPa are binned against BI, using the 10-yr daily-mean outputs between 10°S and 10°N over the ocean (Fig. 14). The binning process is made for the samples where the vertical-mean cumulus heating is more than $2\,\mathrm{K\,day^{-1}}$ to exclude the cases of too-weak convective activity.

The cooling by the snow melting is very strong for smaller BIs and becomes weak along with BI, as was expected. The radiative cooling is very weak for smaller BIs and becomes very strong for larger BIs, since a shallower cloud top with higher temperature emanates more radiative energy upward. The reevaporation of the precipitation does not show a large sensitivity to BI. Figure 14d shows the sum of the heating by the liquid–ice transition, radiation, and reevaporation. It shows greater cooling for both the smaller and larger BIs. The cooling becomes moderate when BI is around 0.5.

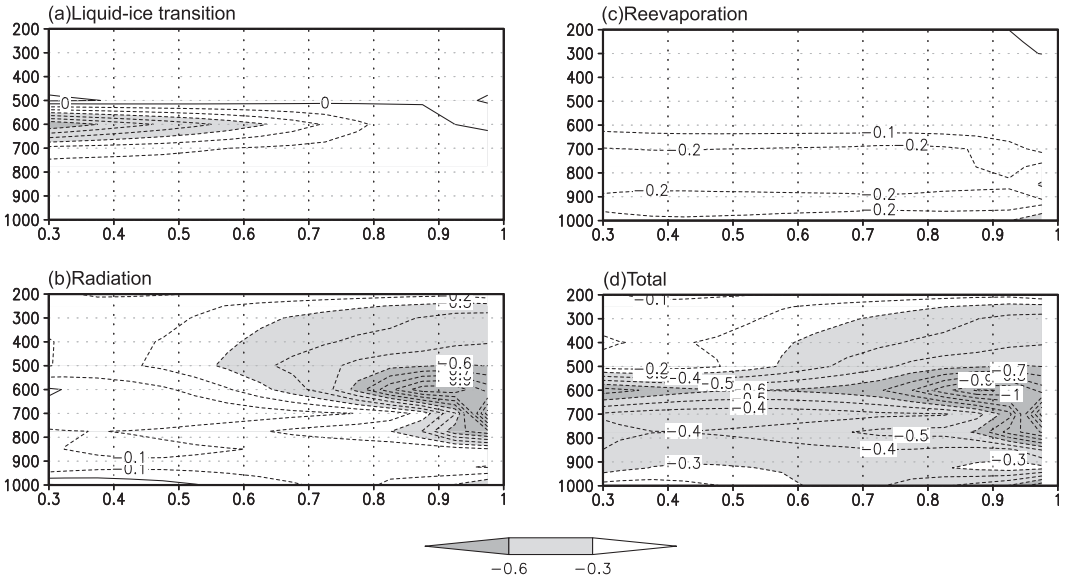

FIG. 14. The heating by (a) liquid–ice transition, (b) radiation, and (c) reevaporation of precipitation normalized by the vertical-mean cumulus heating from 100 to 850 hPa, binned against BI between 10°S and 10°N over the ocean. (d) Total of (a)–(c). Contour intervals are 0.1. The abscissa is BI.

Interestingly, the mean BI between days −5 and 5 calculated from the composited cumulus heating in the model is 0.51. It means that the heating profile in the mature phase is the most efficient one in moderating the cooling by both the snow melting and radiation, suggesting that a vertical mode that maximizes the moistening of the free troposphere is selected. Note that although the mean BI for the cumulus heating in the mature phase is 0.51, the total diabatic heating includes that by the large-scale condensation, which is more top heavy and similar to that of the reanalysis (see Fig. 15b in Part I).

Although this model cannot represent the tilted structure of the diabatic heating, the observation and reanalysis shows a more top-heavy heating profile in the decay phase of the MJO. For the top-heavy heating profile, Fig. 14 shows the reduction of the radiative cooling in the entire free troposphere and the enhancement of the cooling by the snow melting in the middle troposphere, which leads to the moistening of the upper troposphere and the drying of the middle troposphere. It partly explains the tilted structure of the moisture in the decay phase of the MJO. Besides, the cooling by the snow melting in the middle troposphere is considered to be the primary factor in the negative temperature anomaly of the middle troposphere in the decay phase.

The role of shallow convection and congestus clouds in the life cycle of the MJO has been often recognized as preconditioning—that is, moistening of the lower troposphere preceding the deep convection. However, the above discussion suggests that its role is not limited to the preconditioning, but the enhanced activity of the congestus clouds prevents the heating profile from becoming top heavy and thereby plays an important role in augmenting the lower-tropospheric humidity even in the mature phase. This view is more consistent with the concept of the moisture mode, which maintains the existence of instability through the amplification of moisture by the column process rather than the discharge–recharge mechanism, which simply argues the importance of a gradual increase of moisture due to shallow convection prior to deep convection.

A question arises as to why the congestus clouds are enhanced together with the deep convection in the mature phase. One can expect that the cloud top tends to be higher given the moister environment and its entrainment. Figure 15a is the correlation of the cumulus detrainment mass flux with that at 300 hPa averaged over the convective area (15°S–5°N, days −5 to 5). Note that the calculation was made against the daily-mean output. The high positive value at 600 hPa means that the congestus clouds tend to occur collocated with the deep convection. From 850 to 700 hPa, the correlation is small but still positive. Interestingly, it is not that the shallow convection tends to occur when the deep convection is suppressed as is often understood. Figure 15b shows the composited equivalent potential temperature inside cumuli for the highest cloud type and the large-scale mean saturation equivalent potential temperature

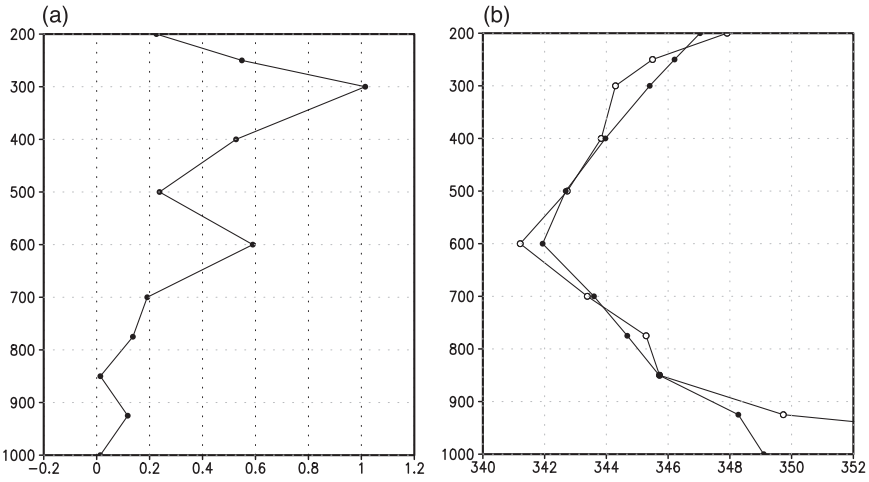

FIG. 15. (a) Correlation of the cumulus detrainment mass flux with that at 300 hPa averaged over the convective area (15°S–5°N, days −5 to 5). (b) Composited in-cloud equivalent potential temperature for the highest cloud type (closed circles) and large-scale mean saturation equivalent potential temperature averaged from days −5 to 5 (open circles).

averaged from days −5 to 5 (denoted as $\hat{\theta}_e$ and θ_e^*, respectively). It shows that even over the convective area, $\hat{\theta}_e$ and θ_e^* profiles are close; that is, the atmosphere is marginally unstable against the highest cloud type. In this condition, the other cloud types with larger entrainment rates tend to lose their buoyancy before reaching the upper troposphere, which should lead to the increased detrainment mass flux in the middle and lower troposphere. If $\hat{\theta}_e$ and θ_e^* were more separated, such cloud types would obtain more buoyancy and tend to reach upper levels, as is often seen in continental deep convection.

5. Discussion

a. Geographical distribution of α

The previous section revealed the importance of α in the development of the MJO. Figure 16 shows the annual-mean α in the lower troposphere calculated from monthly-mean θ and q in the model and reanalysis. Since the potential temperature field is almost horizontally uniform in the tropical free troposphere, the horizontal distribution of α mostly corresponds to the vertical gradient of the moisture. As is expected from

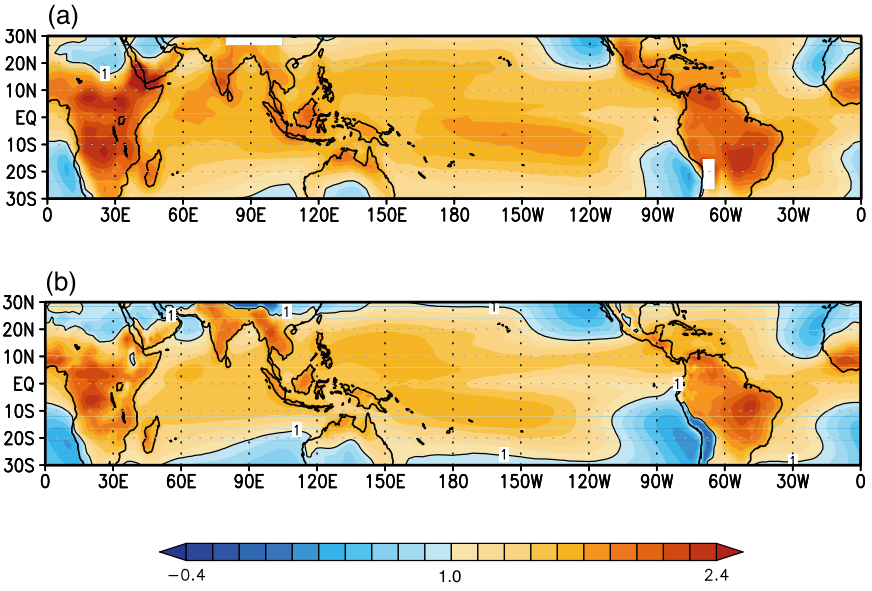

FIG. 16. Annual-mean α averaged from 850 to 700 hPa calculated from the monthly-mean θ and q in (a) the model and (b) the ERA-Interim.

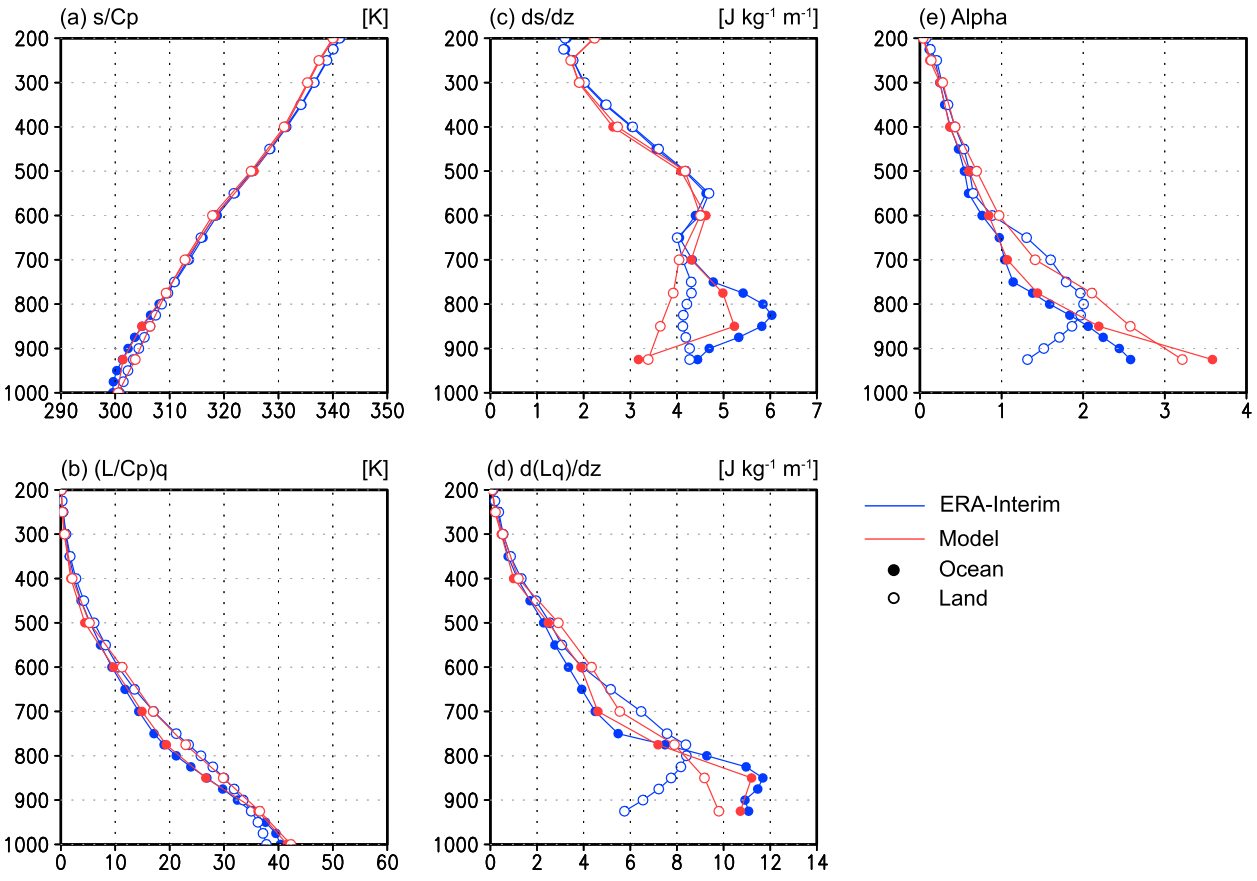

FIG. 17. Annual-mean (a) dry static energy, (b) specific humidity, (c) vertical gradient of the dry static energy, (d) vertical gradient of the specific humidity, and (e) α calculated from the monthly-mean temperature and specific humidity, averaged over the ocean (closed circles) and land (open circles) separately between 10°S and 10°N in the ERA-Interim (blue) and the model (red). The units are (a),(b) K and (c),(d) J kg^{-1} m^{-1}.

(16), α is larger than 1 in the lower troposphere over the tropics. Moreover, it has large values over land such as Africa, South America, and the Maritime Continent. That is, the downward environmental vertical velocity anomaly in the lower troposphere of the convective area seen in Fig. 8c efficiently dries the continental lower troposphere. This is an unfavorable condition for the development of the MJO and appears to explain the suppression of the convective activity of the MJO there.

Figure 17 shows the annual-mean vertical profiles of the dry static energy, specific humidity, their vertical gradients, and α averaged over the ocean and land separately between 10°S and 10°N in both the model and reanalysis. Over land, α is larger only between 600 and 850 hPa. The difference from the ocean reaches 0.7, which is quite a large value and should greatly change the moistening process there. The reason for the difference is attributed to both the greater and weaker vertical gradients of the moisture and dry static energy, respectively, over land (Figs. 17c and 17d). The greater vertical gradient of the moisture is due to the greater amount of the moisture around 800 hPa, which is considered to be caused by shallow convection preceding peak precipitation in the diurnal variation. The smaller vertical gradient of the dry static energy is due to the larger temperature around 900 hPa, which is presumably caused by active growth of a convective boundary layer.

The relation of α to the seasonal and interannual variation of the MJO is an interesting subject and left for future studies.

b. Enhancement of congestus clouds

The previous section pointed out that the lack of large buoyancy is a favorable condition for the enhancement of the congestus clouds. It reduces the population of the deep convection and the cooling by the snow melting, which results in the enhanced moistening in the middle troposphere. The model result appears to be consistent with an observational study of Morita et al. (2006),

which showed that relatively moderate cloud-top height is dominant in the mature phase of the MJO, while very tall convection increases in the suppressed phase. They also demonstrated that lightning frequency decreases in the mature phase, which suggests the occurrence of more moderate convection.

A plausible reason for the small instability in the mature phase is the quasi-stationary feature of the MJO. In the case of continental deep convection, large buoyancy is rapidly generated by the strong heating of the surface. Even over the ocean, certain types of equatorial waves such as gravity and Kelvin waves involve rapid changes in free-tropospheric temperature as an essential feature of the waves. In their cooling phases, relatively large buoyancy can be dynamically induced. In the case of the MJO, the temperature profile is almost horizontally uniform and does not change significantly. In addition, according to a linear theory, anomalous large-scale vertical velocity is in proportion to the horizontal wavenumber squared (e.g., Kuang 2008, 2011). Thereby, upward vertical velocity becomes weaker for waves with smaller horizontal wavenumbers such as the MJO, which gives a weaker large-scale forcing and the lack of large buoyancy. This fact also means that the smaller horizontal wavenumber is convenient for the growth of the free-tropospheric humidity and explains why the MJO prefers the smaller wavenumber.

There are other possibilities. Since frictional convergence in the boundary layer induces upward motion on the top of the layer, it might cause larger destabilization in the lower troposphere and lead to the enhancement of the middle and shallow convection. If this is the case, the frictional convergence has a unique role in the context of the moisture mode and might justify the frictional-convergence theory of the MJO (Wang 1988; Salby and Hendon 1994) to some extent. In addition, since the increased reevaporation of the precipitation over the convective area causes the anomalous cooling in the lower troposphere, it must be compensated by the enhanced cumulus subsidence or the reduction in the large-scale upward motion. If the former is the case, the reevaporation of precipitation also causes the enhancement.

This study suggests a necessary condition for theoretical models to produce the MJO: moistening in the lower troposphere must be enhanced in the mature phase of the MJO. Kuang (2008) and Andersen and Kuang (2008) developed a linear simple model of the tropical atmosphere with two vertical modes where the depth of convection depends on free-tropospheric humidity. The model succeeded in representing and understanding various equatorial waves. In addition, a moisture mode was included in their model. However, it was stable. One of the reasons is considered to be in their formulation that the deep convection occurring in the moist condition quickly dries the atmosphere and thereby suppresses its own activity. However, the analysis of this study suggests that the moistening of the free troposphere can be enhanced even in moist condition if large-scale forcing is weak, the population of congestus clouds is large, and the cooling of snow melting is reduced.

It is also suggested that the reason for the success of the CS scheme in better representing the MJO is that the scheme produces more congestus clouds even when the free troposphere is moist. Chikira and Sugiyama (2010) examined the scheme's behavior against the free-tropospheric humidity and showed that the entrainment formulation of Gregory (2001) used in this study produces more heating in the lower troposphere under the moist environment, while the other formulation by Neggers et al. (2002) gives more top-heavy heating. The AGCM experiment with the latter formulation did not show a strong signal of the MJO in the power spectrum, but those of the other high-frequency waves were greater. This result supports the above idea that the enhancement of moistening under the moist environment is important for the MJO, but its suppression is necessary for the other high-frequency waves.

Some AGCMs succeeded in representing MJO-like waves by applying a threshold for destabilization rates by a large-scale forcing (e.g., Zhang and Mu 2005; Deng and Wu 2010). This method prevents deep convection and gives more shallow convection when the large-scale forcing is weak. Since the forcing of MJO is weak, it should give more shallow convection in the mature phase of the MJO-like waves, which might explain the success of this method.

The shallow convection detraining around 850 hPa is not enhanced in this model prior to or during the mature phase of the MJO-like waves (Fig. 10b). However, since the model appears to underestimate its activity (Part I), this is considered to be an issue to be updated in the future. The underestimation of this shallow convection might be a reason for the weaker westward tilting of the humidity field. Despite the slight westward tilting of the humidity, the model diabatic heating does not show any hint of tilting (Part I). The reason is unclear and beyond the scope of this study.

c. Relation to column moist static energy analysis

The prognostic equation for column-integrated MSE is written as

$$\left\langle \frac{\partial h}{\partial t} \right\rangle = -\langle \boldsymbol{v}_h \cdot \nabla h \rangle - \left\langle \omega \frac{\partial h}{\partial p} \right\rangle + F_h + \langle Q_r \rangle + \langle Q_i \rangle, \tag{18}$$

where the angle brackets are redefined to represent vertical integrals from the surface to the top of the troposphere and F_h denotes surface MSE flux. The variation of the column MSE provides a measure of column moisture under the WTG balance.

An advantage of the analytical method proposed in this study over the use of the column MSE is that it makes it possible to focus on moisture variation at specific levels such as the lower troposphere, which is considered to have a primary importance for deep convection. One might assume that the variation of the column MSE is a measure of the lower-tropospheric humidity variation because 1) the moisture in the boundary layer is mostly determined by surface temperature and thereby cannot change significantly and 2) the amount of upper-tropospheric moisture is much smaller than that in the lower troposphere and does not contribute to the column MSE. This will be true to some extent, but its accuracy is not enough to treat some problems, as discussed below. The method of this study provides an accurate way of understanding moisture variation at specific levels.

The effect of cloud process is eliminated in (18) except for Q_i, since that of cumulus convection and vapor–liquid transition never change the column MSE. On the other hand, (13) exhibits how various subprocesses work on the moisture variation. This is useful for understanding how each component of cloud schemes affect the variation.

Some of the concluding remarks in this study are derived from (18) as well. Both (13) and (18) show that the radiative warming anomaly moistens and the cooling by the liquid–ice transition dries the atmosphere. This study concluded that the top-heavy heating profile in the mature phase is an unfavorable condition for maintaining the lower-tropospheric humidity. As is pointed out by, for example, Peters et al. (2008), the second term in the right-hand side of (18) also shows that the column MSE increases more for larger upward vertical velocity in the lower troposphere (it corresponds to more heating there), given a positive sign of $\partial h/\partial p$ there. If the ω profile is top heavy, it tends to decrease the column MSE, given a negative sign of $\partial h/\partial p$ in the upper troposphere. Kuang (2011) showed the importance of this effect in the scale selection of the MJO.

This study gives a different view of the effect of the vertical moisture gradient in the lower troposphere on the development of the MJO from the column MSE analysis. In the second term of the right-hand side of (18), if $\partial q/\partial p$ is larger in the lower troposphere (it corresponds to larger $\partial h/\partial p$ there), then it enhances the increase in the column MSE with negative values of ω, which will be interpreted as a favorable condition for the development of the MJO. According to this study, however, the anomalous environmental vertical velocity is downward in the lower troposphere of the convective area, and thereby the larger $\partial q/\partial p$ leads to more drying there. Since the lower-tropospheric humidity has a primary importance for a deep convective activity, it is an unfavorable condition for the development of the MJO. Although it is true that larger $\partial q/\partial p$ leads to an increase in the column moisture, it does not necessarily result in a moisture increase in the lower-tropospheric counterpart. The difference of the views appears to come from different responses between the column and lower-tropospheric moisture to the increased $\partial q/\partial p$. This is an example of how the method of this study provides an accurate view for some problems.

Although this study supports the moisture-mode theory in the sense that an instability exists through the amplification of free-tropospheric humidity, it is still unclear whether the instability depicted in this study is the same as that given by the theories based on the column moisture. At the least, the above discussion shows that a formulation based on the column moisture can give a wrong answer to some problems. It will be a subject of future studies to improve such theories so that it gives a correct response to the basic state where the instability develops.

The enhancement of surface evaporation interacting with the surface wind component of MJO has been recognized to play an important role (Emanuel 1987; Neelin et al. 1987) in the waves. The influence of the surface flux on the column moisture is clearly depicted in (18). However, the method of this study does not directly show how the surface flux affects the free-tropospheric humidity profile. Although the effect of the surface flux on the properties of the overlying boundary layer is easily understood, it depends on the type of subsequent convection how the change in the boundary layer affects the lower-tropospheric humidity. If deep (shallow) convection is enhanced, it should lead to the drying (moistening) of the lower troposphere. This subject needs a careful examination and is left for future studies.

6. Summary and conclusions

The eastward-propagating intraseasonal oscillation represented by the Chikira–Sugiyama cumulus scheme was investigated focusing on the variation of the free-tropospheric humidity. The composited fields show that the WTG balance is well satisfied. The net effect of the vertical advection and cloud process moistens the free troposphere. In particular, it enhances the positive moisture anomaly over the convective area of the MJO-like waves, supporting the concept of the moisture-mode theory. The horizontal advection dries the free

troposphere. The drying is enhanced over the western margin of the convective area and slightly weakened over the eastern margin, thereby causing the eastward propagation of the moisture field in cooperation with the amplification of the positive moisture anomaly by the column process.

The horizontal advection by the slow fields shows the enhanced drying over the western margin of the convective area and the anomalous moistening over the eastern margin. The advection of the drier air by the stronger westerly wind on the western side of the convective area leads to the significant drying on the western side and anomalous moistening on the eastern side. The equatorward wind of the Rossby wave circulation accompanying the convective heating reinforces it by transporting dry air from the extratropics into the western side. The weak poleward wind of the circulation on the eastern side also appears to contribute to the moistening there. The high-frequency waves tend to strongly dry the interior of the convective area and slightly moisten its margins, which has a role similar to diffusion or damping.

The moisture variation is well understood by introducing the environmental vertical velocity defined by the sum of large-scale mean vertical velocity and cumulus subsidence. The velocity is determined by a thermodynamic balance under the WTG balance. In the upper troposphere over the convective area, the enhanced large-scale condensation and radiative warming anomaly lead to the strong upward environmental vertical velocity anomaly. In the lower troposphere, the enhanced evaporative cooling of the cloud and precipitation is larger than the radiative warming anomaly, resulting in the weak downward environmental vertical velocity anomaly.

By eliminating the environmental vertical velocity in the set of the equations for moisture and potential temperature, an equation for slowly varying moisture is obtained. A nondimensional parameter α defined by the vertical gradient of moisture divided by that of potential temperature appears as a controlling factor in the equation, which characterizes the efficiency of moistening (drying) by the upward (downward) environmental vertical velocity induced by external heating (cooling). The parameter α represents 1) the effect of static stability on the environmental vertical velocity through the thermodynamic balance and 2) the effect of vertical moisture gradient on the environmental vertical advection. Larger (smaller) static stability reduces (enhances) the absolute values of the environmental vertical velocity, while a larger (smaller) vertical moisture gradient enhances (reduces) either the moistening or drying by the upward or downward environmental vertical advection, respectively. It is found that α gives useful information on how given profiles of temperature and moisture affect the moisture tendency under the WTG balance.

In the lower troposphere over the convective area, the primary moistening factor is the decrease in α that is caused by the moistening in the middle troposphere. The radiative warming anomaly is the major contributor to the moistening of the middle troposphere through the enhancement of the upward environmental vertical velocity anomaly. Secondarily, the vertical moisture transport by the high-frequency waves and the evaporation of the detraining cloud water reinforce it. The melting of snow significantly cools and thereby dries the middle troposphere. The reevaporation of precipitation in the lower troposphere works as a drying factor because its cooling effect induces the downward environmental vertical velocity whose drying effect overcomes the direct moistening effect of the reevaporation. The large-scale condensation in the upper troposphere works as drying, since the drying effect through the removal of the moisture overcomes the moistening effect through the upward environmental vertical velocity anomaly. Whether the condensation and evaporation work as moistening or drying depends on the sign of the vertical gradient of moist static energy.

A strongly top-heavy heating profile is an unfavorable condition for moistening the free troposphere, since it gives more cooling by snow melting in the middle troposphere, which leads to drying there. On the other hand, a strongly bottom-heavy profile gives enhanced radiative cooling, which is also an unfavorable condition. The cooling by the sum of the snow melting and radiation is minimized at a certain point between these two extreme cases. The profile in the mature phase of the model MJO-like waves is the most efficient in moistening the free troposphere, suggesting that a vertical mode that maximizes the moistening is selected.

The cause of the enhancement of the congestus clouds in the mature phase was examined. The atmosphere is marginally unstable even over the convective center, which is a favorable condition for middle and shallow convection. This feature is consistent with an observational study and considered to be the result of the quasi-stationary feature of the MJO. Other possibilities include the role of frictional convergence and the evaporative cooling of precipitation in destabilizing the lower troposphere.

The spatial distribution of the lower-tropospheric α exhibits large values over land. That is, the lower troposphere is efficiently dried by the downward environmental vertical velocity anomaly there. This is an unfavorable condition for the development of the MJO

and thus appears to explain the suppression of the convective activity of the MJO over land.

The analytical method proposed in this study provides accurate understanding of slowly changing moisture variation in the free troposphere. It can be also used for the analyses of the other phenomena, if the WTG balance is satisfied there. Unlike the column MSE analysis, it is possible to focus on specific levels such as the lower troposphere. Additionally, it is helpful to figure out the roles of subdivided components of cloud processes. This study shows that a larger vertical gradient of lower-tropospheric moisture is an unfavorable condition for the development of the MJO, which disagrees with the implication of the column MSE analysis.

Acknowledgments. I am grateful for valuable comments from Masahiro Sugiyama and three anonymous reviewers. A discussion with Professor David A. Randall greatly improved this manuscript. The ERA-Interim data were obtained from the ECMWF data server. The computations were performed with the Earth Simulator in JAMSTEC.

APPENDIX

Moist Static Energy Equation

Applying WTG approximation, the prognostic equation for dry static energy is given by

$$w\frac{\partial s}{\partial z} = Q_{\mathrm{cu}} + L_v(\tilde{C} - \tilde{R}_v) + Q_r + \tilde{Q}_i + Q_{\mathrm{df}}.$$

Decomposing Q_{cu} into detrainment and subsidence terms and neglecting the detrainment, the above equation becomes

$$\tilde{w}\frac{\partial s}{\partial z} = L_v(\tilde{C} - \tilde{R}_v) + Q_r + \tilde{Q}_i + Q_{\mathrm{df}}.$$

Assuming

$$\tilde{w}\frac{\partial s}{\partial z} \simeq \langle\tilde{w}\rangle\frac{\partial\langle s\rangle}{\partial z}, \tag{A1}$$

and dividing the equation by $\partial\langle s\rangle/\partial z$,

$$\langle\tilde{w}\rangle \simeq [L_v(\tilde{C} - \tilde{R}_v) + Q_r + \tilde{Q}_i + Q_{\mathrm{df}}]\left(\frac{\partial\langle s\rangle}{\partial z}\right)^{-1} \tag{A2}$$

is obtained.

The prognostic equation for MSE by the column process is given by

$$\left(\frac{\partial h}{\partial t}\right)_{\mathrm{col}} = -w\frac{\partial h}{\partial z} + \left(\frac{\partial h}{\partial t}\right)_{\mathrm{cu}} + Q_r + \tilde{Q}_i + Q_{\mathrm{df}} + L_v S_{\mathrm{df}},$$

where $(\partial h/\partial t)_{\mathrm{cu}}$ denote an MSE tendency by the subgrid-scale cumulus effect. The decomposition of the cumulus effect into the detrainment and subsidence terms leads to

$$\left(\frac{\partial h}{\partial t}\right)_{\mathrm{col}} = -\tilde{w}\frac{\partial h}{\partial z} + D_h + Q_r + \tilde{Q}_i + Q_{\mathrm{df}} + L_v S_{\mathrm{df}},$$

where D_h is an MSE source by the detrainment. The use of

$$\tilde{w}\frac{\partial h}{\partial z} \simeq \langle\tilde{w}\rangle\frac{\partial\langle h\rangle}{\partial z} + L_v S_{\mathrm{hf}},$$

(A2), and (16) leads to

$$\left(\frac{\partial h}{\partial t}\right)_{\mathrm{col}} = (\alpha - 1)L_v(\tilde{C} - \tilde{R}) + \alpha(Q_r + \tilde{Q}_i + Q_{\mathrm{df}}) + D_h + L_v(S_{\mathrm{df}} + S_{\mathrm{hf}}),$$

which is almost identical to (13).

REFERENCES

Andersen, J. A., and Z. Kuang, 2008: A toy model of the instability in the equatorially trapped convectively coupled waves on the equatorial beta plane. *J. Atmos. Sci.,* **65,** 3736–3757.

——, and ——, 2012: Moist static energy budget of MJO-like disturbances in the atmosphere of a zonally symmetric aquaplanet. *J. Climate,* **25,** 2782–2804.

Arakawa, A., and W. H. Schubert, 1974: Interaction of a cumulus cloud ensemble with the large-scale environment, Part I. *J. Atmos. Sci.,* **31,** 674–701.

Back, L. E., and C. S. Bretherton, 2006: Geographic variability in the export of moist static energy and vertical motion profiles in the tropical Pacific. *Geophys. Res. Lett.,* **33,** L17810, doi:10.1029/2006GL026672.

Benedict, J. J., and D. A. Randall, 2007: Observed characteristics of the MJO relative to maximum rainfall. *J. Atmos. Sci.,* **64,** 2332–2354.

Bladé, I., and D. L. Hartmann, 1993: Tropical intraseasonal oscillations in a simple nonlinear model. *J. Atmos. Sci.,* **50,** 2922–2939.

Brown, R. G., and C. Zhang, 1997: Variability of midtropospheric moisture and its effect on cloud-top height distribution during TOGA COARE. *J. Atmos. Sci.,* **54,** 2760–2774.

Chikira, M., 2010: A cumulus parameterization with state-dependent entrainment rate. Part II: Impact on climatology in a general circulation model. *J. Atmos. Sci.,* **67,** 2194–2211.

——, and M. Sugiyama, 2010: A cumulus parameterization with state-dependent entrainment rate. Part I: Description and sensitivity to temperature and humidity profiles. *J. Atmos. Sci.,* **67,** 2171–2193.

——, and ——, 2013: Eastward-propagating intraseasonal oscillation represented by Chikira–Sugiyama cumulus parameterization. Part I: Comparison with observation and reanalysis. *J. Atmos. Sci.,* **70,** 3920–3939.

Deng, L., and X. Wu, 2010: Effects of convective processes on GCM simulations of the Madden–Julian oscillation. *J. Climate,* **23,** 352–377.

Derbyshire, S. H., I. Beau, P. Bechtold, J.-Y. Grandpeix, J.-M. Piriou, J.-L. Redelsperger, and P. M. M. Soares, 2004: Sensitivity of moist convection to environmental humidity. *Quart. J. Roy. Meteor. Soc.,* **130,** 3055–3079.

Emanuel, K. A., 1987: An air-sea interaction model of intraseasonal oscillations in the tropics. *J. Atmos. Sci.,* **44,** 2324–2340.

Fuchs, Ž., and D. J. Raymond, 2002: Large-scale modes of a nonrotating atmosphere with water vapor and cloud–radiation feedbacks. *J. Atmos. Sci.,* **59,** 1669–1679.

——, and ——, 2005: Large-scale modes in a rotating atmosphere with radiative–convective instability and WISHE. *J. Atmos. Sci.,* **62,** 4084–4094.

Grabowski, W. W., 2003: MJO-like coherent structures: sensitivity simulations using the cloud-resolving convection parameterization (CRCP). *J. Atmos. Sci.,* **60,** 847–864.

——, and M. W. Moncrieff, 2004: Moisture–convection feedback in the tropics. *Quart. J. Roy. Meteor. Soc.,* **130,** 3081–3104.

Gregory, D., 2001: Estimation of entrainment rate in simple models of convective clouds. *Quart. J. Roy. Meteor. Soc.,* **127,** 53–72.

Hannah, W. M., and E. D. Maloney, 2011: The role of moisture–convection feedbacks in simulating the Madden–Julian oscillation. *J. Climate,* **24,** 2754–2770.

Hu, Q., and D. A. Randall, 1994: Low-frequency oscillations in radiative-convective systems. *J. Atmos. Sci.,* **51,** 1089–1099.

Kemball-Cook, S. R., and B. C. Weare, 2001: The onset of convection in the Madden–Julian oscillation. *J. Climate,* **14,** 780–793.

Kim, D., A. H. Sobel, A. D. Del Genio, Y. Chen, S. J. Camargo, M.-S. Yao, M. Kelley, and L. Nazarenko, 2012: The tropical subseasonal variability simulated in the NASA GISS general circulation model. *J. Climate,* **25,** 4641–4659.

Kiranmayi, L., and E. D. Maloney, 2011: Intraseasonal moist static energy budget in reanalysis data. *J. Geophys. Res.,* **116,** D21117, doi:10.1029/2011JD016031.

Kuang, Z., 2008: A moisture–stratiform instability for convectively coupled waves. *J. Atmos. Sci.,* **65,** 834–854.

——, 2010: Linear response functions of a cumulus ensemble to temperature and moisture perturbations and implication to the dynamics of convectively coupled waves. *J. Atmos. Sci.,* **67,** 941–962.

——, 2011: The wavelength dependence of the gross moist stability and the scale selection in the instability of column-integrated moist static energy. *J. Atmos. Sci.,* **68,** 61–74.

Lin, C.-C., and A. Arakawa, 1997: The macroscopic entrainment processes of simulated cumulus ensemble. Part II: Testing the entraining-plume model. *J. Atmos. Sci.,* **54,** 1044–1053.

Lin, J.-L., and Coauthors, 2006: Tropical intraseasonal variability in 14 IPCC AR4 climate models. Part I: Convective signals. *J. Climate,* **19,** 2665–2690.

Madden, R. A., and P. R. Julian, 2005: Historical perspective. *Intraseasonal Variability in the Atmosphere-Ocean Climate System,* W. K.-M. Lau and D. E. Waliser, Eds., Praxis, 1–18.

Maloney, E. D., 2009: The moist static energy budget of a composite tropical intraseasonal oscillation in a climate model. *J. Climate,* **22,** 711–729.

——, and D. L. Hartmann, 1998: Frictional moisture convergence in a composite life cycle of the Madden–Julian oscillation. *J. Climate,* **11,** 2387–2403.

——, and ——, 2001: The sensitivity of intraseasonal variability in the NCAR CCM3 to changes in convective parameterization. *J. Climate,* **14,** 2015–2034.

——, A. H. Sobel, and W. M. Hannah, 2010: Intraseasonal variability in an aquaplanet general circulation model. *J. Adv. Model Earth Syst.,* **2** (5), doi:10.3894/JAMES.2010.2.5.

Morita, J., Y. N. Takayabu, S. Shige, and Y. Kodama, 2006: Analysis of rainfall characteristics of the Madden–Julian oscillation using TRMM satellite data. *Dyn. Atmos. Oceans,* **42,** 107–126, doi:10.1016/j.dynatmoce.2006.02.002.

Neelin, J. D., and I. M. Held, 1987: Modeling tropical convergence based on the moist static energy budget. *Mon. Wea. Rev.,* **115,** 3–12.

——, ——, and K. H. Cook, 1987: Evaporation-wind feedback and low-frequency variability in the tropical atmosphere. *J. Atmos. Sci.,* **44,** 2341–2348.

Neggers, R. A. J., A. P. Siebesma, and H. J. J. Jonker, 2002: A multiparcel method for shallow cumulus convection. *J. Atmos. Sci.,* **59,** 1655–1668.

Numaguti, A., R. Oki, K. Nakamura, K. Tsuboki, N. Misawa, T. Asai, and Y.-M. Kodama, 1995: 4-5-day-period variation and low-level dry air observed in the equatorial western Pacific during the TOGA-COARE IOP. *J. Meteor. Soc. Japan,* **73,** 267–290.

Peters, M. E., Z. Kuang, and C. Walker, 2008: Analysis of atmospheric energy transport in ERA-40 and implications for simple models of the mean tropical circulation. *J. Climate,* **21,** 5229–5241.

Raymond, D. J., 2001: A new model of the Madden–Julian oscillation. *J. Atmos. Sci.,* **58,** 2807–2819.

——, and Ž. Fuchs, 2009: Moisture modes and the Madden–Julian oscillation. *J. Climate,* **22,** 3031–3046.

Redelsperger, J.-L., D. B. Parsons, and F. Guichard, 2002: Recovery processes and factors limiting cloud-top height following the arrival of a dry intrusion observed during TOGA COARE. *J. Atmos. Sci.,* **59,** 2438–2457.

Salby, M. L., and H. H. Hendon, 1994: Intraseasonal behavior of clouds, temperature, and motion in the tropics. *J. Atmos. Sci.,* **51,** 2207–2224.

Sherwood, S. C., 1999: Convective precursors and predictability in the tropical western Pacific. *Mon. Wea. Rev.,* **127,** 2977–2991.

Siebesma, A. P., and J. W. M. Cuijpers, 1995: Evaluation of parametric assumptions for shallow cumulus convection. *J. Atmos. Sci.,* **52,** 650–666.

Slingo, J. M., and Coauthors, 1996: Intraseasonal oscillations in 15 atmospheric general circulation models: Results from an AMIP diagnostic subproject. *Climate Dyn.,* **12,** 325–357.

Sobel, A., and J. D. Neelin, 2006: The boundary layer contribution to intertropical convergence zones in the quasi-equilibrium tropical circulation model framework. *Theor. Comput. Fluid Dyn.,* **20,** 323–350, doi:10.1007/s00162-006-0033-y.

——, and E. Maloney, 2012: An idealized semi-empirical framework for modeling the Madden–Julian oscillation. *J. Atmos. Sci.,* **69,** 1691–1705.

——, and ——, 2013: Moisture modes and the eastward propagation of the MJO. *J. Atmos. Sci.,* **70,** 187–192.

——, J. Nilsson, and L. M. Polvani, 2001: The weak temperature gradient approximation and balanced tropical moisture waves. *J. Atmos. Sci.,* **58,** 3650–3665.

Sugiyama, M., 2009a: The moisture mode in the quasi-equilibrium tropical circulation model. Part I: Analysis based on the weak temperature gradient approximation. *J. Atmos. Sci.,* **66,** 1507–1523.

——, 2009b: The moisture mode in the quasi-equilibrium tropical circulation model. Part II: Nonlinear behavior on an equatorial β plane. *J. Atmos. Sci.,* **66,** 1525–1542.

Thayer-Calder, K., and D. A. Randall, 2009: The role of convective moistening in the Madden–Julian oscillation. *J. Atmos. Sci.,* **66,** 3297–3312.

Tompkins, A. M., 2001: Organization of tropical convection in low vertical wind shears: The role of water vapor. *J. Atmos. Sci.,* **58,** 529–545.

Tulich, S. N., and B. E. Mapes, 2010: Transient environmental sensitivities of explicitly simulated tropical convection. *J. Atmos. Sci.,* **67,** 923–940.

Wang, B., 1988: Dynamics of tropical low-frequency waves: An analysis of the moist Kelvin wave. *J. Atmos. Sci.,* **45,** 2051–2065.

Watanabe, M., and Coauthors, 2010: Improved climate simulation by MIROC5: Mean states, variability, and climate sensitivity. *J. Climate,* **23,** 6312–6335.

Zhang, C., 2005: Madden-Julian Oscillation. *Rev. Geophys.,* **43,** RG2003, doi:10.1029/2004RG000158.

Zhang, G. J., and M. Mu, 2005: Simulation of the Madden–Julian oscillation in the NCAR CCM3 using a revised Zhang–McFarlane convection parameterization scheme. *J. Climate,* **18,** 4046–4064.